Hindawi
International Journal of Energy Research
Volume 2023, Article ID 3684046, 23 pages
https://doi.org/10.1155/2023/3684046

*Research Article*

# $CO_2$ Impact on Methane Pyrolysis as a Key Issue of Using Biogas as an Educt: A Theoretical Study

**Inés Durán,[1] Benjamin Dietrich,[2] Christoph Hofberger,[1] Leonid Stoppel,[1] Neele Uhlenbruck,[1] and Thomas Wetzel[1,2]**

[1]*Karlsruhe Liquid Metal Laboratory (KALLA), Institute for Thermal Energy Technology and Safety (ITES), Karlsruhe Institute of Technology (KIT), 76344 Eggenstein-Leopoldshafen, Germany*
[2]*Institute of Thermal Process Engineering (TVT), Karlsruhe Institute of Technology (KIT), 76131 Karlsruhe, Germany*

Correspondence should be addressed to Inés Durán; ines.duran@kit.edu

Received 20 February 2023; Revised 14 October 2023; Accepted 18 October 2023; Published 6 December 2023

Academic Editor: Juan M. Coronado



Dry reforming of methane (DRM) has attracted great interest for the production of syngas and/or hydrogen in a more environmentally friendly way. It is especially advantageous in this case to use biogas—as a mixture of methane, $CO_2$, and traces of further gases—as a feedstock replacement for natural gas. Nevertheless, industrial implementation of DRM is currently limited because of its inherent process restrictions. The biggest challenge of dry reforming is the deposition of carbon on the catalyst, known as "coking." The focus of this theoretical study is to evaluate the feasibility of a biogas dry reforming process in a liquid metal (Sn) bubble column reactor. This technology has already been proven suitable for methane pyrolysis to obtain hydrogen, preventing issues related to reactor clogging or catalyst deactivation caused by carbon deposition. Results show that at high operating temperatures and atmospheric pressure, a product gas primarily composed of $H_2$ and CO would be obtained. $CO_2$ and water vapor may also be present in the final product depending on the operating conditions. The molten tin inside the reactor would, according to the presented theoretical considerations, not be affected by the formation of carbides and oxides. Additionally, the syngas composition (the $H_2:CO$ ratio) could be adjusted by using different $CH_4:CO_2$ feed ratios.

## 1. Introduction

In the dry reforming of methane (DRM) process, $CH_4$ and $CO_2$ react to form a synthesis gas, a mixture of CO and $H_2$. This synthesis gas, commonly known as "syngas," is a versatile feedstock that can be used to produce a variety of fuels and chemicals, such as methanol, acetic acid, dimethyl ether (DME), and liquid hydrocarbons via the Fischer-Tropsch process.

Currently, syngas is mainly obtained by the steam reforming of methane (SRM) in which $CH_4$ and steam react under additional heat obtaining a gas product with a $H_2$-to-CO ratio of 3 : 1. Frequently, SRM is carried out in combination with the so-called water-gas shift reaction: CO will react further with water to yield $CO_2$ and even more $H_2$.

Instead of producing $CO_2$, DRM utilizes this greenhouse gas to obtain value-added products. Therefore, it seems like an attractive and sustainable technology to convert biogas, a renewable mixture of $CH_4$ and $CO_2$, directly to syngas. Additionally, this would avoid the cost of biogas upgrading since no $CO_2$ separation process is required.

*1.1. Biogas.* Biogas is a renewable energy source obtained from the decomposition of organic matter. It is primarily composed of methane and carbon dioxide along with trace amounts of other components like nitrogen, water vapor, oxygen, hydrogen sulfide, ammonia, and siloxanes. This gas mixture can be transformed to hydrogen and syngas showing great potential as a green alternative to meet environmental goals.

By the end of 2019, about 19,000 biogas plants and 725 biomethane plants were already operating in Europe, producing about 15.8 bcm of biogas and 2.5 bcm of biomethane [1]. According to the estimates of the European Biogas Association (EBA), the growth potential is expected to double by 2030, and combined biogas and biomethane production could reach 95 bcm by 2050.

Biogas composition depends greatly on its source as it can be obtained in very different environments. For instance, sewage digesters typically produce a mixture containing a volumetric fraction of 55–65% methane ($CH_4$), 35–45% carbon dioxide ($CO_2$), and 1% nitrogen ($N_2$), whereas organic waste digesters typically show compositions of 60–70% $CH_4$, 30–40% $CO_2$, and 1% $N_2$, and gas from landfills is made up of 45–55% $CH_4$, 30–40% $CO_2$, and 5 to 15% $N_2$ [2]. Therefore, the ratio of $CH_4$ to $CO_2$ is mainly in the range of 1.0–2.3 [3]. $CH_4$-to-$H_2O$ ratios and $CH_4$-to-$O_2$ ratios in biogas are typically higher than 3 and higher than 20, respectively. Table 1 shows examples of biogas composition depending on the starting source [3].

As shown in Table 1, the concentration of trace compounds in biogas varies greatly depending on the substrate and production route. Usually, biogas is purified from impurities, such as siloxanes and sulfur species, to avoid the frequent replacement of catalysts in a subsequent process like methanol synthesis or biogas reforming [13]. Some biogas mixtures may contain nitrogen, which is an inert gas in biogas reforming, but can increase the energy consumption to reach the desired reaction temperature.

After a cleaning and upgrading process (removal of $CO_2$ and existing impurities), biogas in the form of biomethane can be used as a renewable substitute for natural gas [14]. Methane is a flammable gas, whose flammability limit in air is 5% to 15% by volume [15]. In order to safely transport the biogas through pipelines, it must be ensured that the oxygen content is less than 2%. Hydrogen sulfide must be scrubbed from the gas by carbon filters before it enters the networks and must be <10 ppm. In addition, the $CO_2$ content of the biomethane should be less than 2-5% for pipeline quality, depending on the regulatory frameworks in each country [16].

*1.2. Dry Reforming of Methane.* Biogas can be converted to syngas, which could then be used to obtain high-value-added liquid fuels and chemicals [3]. Different methane-reforming technologies, such as autothermal reforming (ATR), steam reforming (SRM), dry reforming (DRM), or a combination of the latter, are available. SRM essentially employs steam to produce syngas, and ATR uses oxygen (and carbon dioxide and/or steam), while DRM uses carbon dioxide. Of all these processes, DRM is the least favorable from a thermodynamic point of view, although it has the advantage of using carbon dioxide as an oxidant (while all the other processes generate $CO_2$ at some point of the process). Therefore, DRM seems to be a promising sustainable route for the direct conversion of biogas into syngas.

Depending on the target product and stoichiometry of the respective reaction, an optimum molar ratio between hydrogen and carbon monoxide in the synthesis gas is required. Syngas for methanol or hydrocarbon production (via Fischer–Tropsch chemistry) requires a $H_2/CO$ feed ratio of 2 : 1 [17], whereas syngas with $H_2/CO < 1$ is suitable for the synthesis of dimethyl ether [18]. Currently, syngas is mainly produced by SRM or ATR, which yield a $H_2:CO$ ratio of about 3. Methane dry reforming usually results in a ratio close to 1, required for instance for the production of aldehydes by the oxoprocess (hydroformylation). However, several studies [17, 19, 20] have reported that the $H_2$ : CO ratio of syngas produced via biogas dry reforming could be adjust to the desired end-use industrial application by controlling the $CH_4/CO_2$ composition of the feed gas.

*1.2.1. Thermodynamics of Dry Reforming of Methane.* The reaction of $CO_2$ and $CH_4$ is strongly endothermic and usually occurs at temperatures higher than 800°C. This reaction is also affected by the simultaneous occurrence of several side reactions, including the reverse water-gas shift reaction, the $CH_4$ pyrolysis, and the Boudouard reaction (reaction numbers 2, 7, and 8, respectively, in Table 2). The latter two reactions are responsible for carbon deposition (or coking), which is usually a problem as it blocks the surface and causes severe deactivation of the catalyst [21].

He and Liu [18] carried out a thermodynamic analysis of DRM under the following conditions: temperature = 277 − 1227°C, pressure = 0.4 − 12 bar, $CO_2/CH_4$ molar ratio = 1.0 − 10, and $O_2/CO_2$ molar ratio = 0 − 1.0 in the feed. The main reactions involved in DRM according to [18] are shown in Table 2.

The combustion and partial oxidation of methane (reactions 5 and 6, respectively, in Table 2) can be neglected in some cases as they only take place when oxygen is fed to the reforming process. The oxygen content in biogas is usually lower than 1%. However, it can be higher (up to 5%) in landfill gas as it is collected through permeable tubes by providing a slight underpressure [22].

Moreover, oxygen is not produced as a by-product of other reactions. The direct thermal dissociation of $CO_2$ ($CO_2 \rightleftarrows CO + 0.5O_2$) to form carbon monoxide and molecular oxygen occurs only at very high temperatures [23, 24] as shown in Figure 1. Therefore, at 1 bar and less than 1400°C, the thermal dissociation of $CO_2$ is negligible (both due to equilibrium position and slow kinetics).

Water vapor is also an important component in biogas, as it usually leaves the digesters saturated with water [25, 26], so the absolute amount of water depends on the temperature. It can be removed before the reforming process or used as feed gas. If water vapor is also added to the reforming process, a combined $CO_2$ and steam reforming of methane takes place, which is referred to as bireforming or "steam biogas reforming" [3].

Another more recently proposed variation of the reforming process by simultaneously adding $O_2$ is the trireforming of methane (TRM), which is a combination of three methane-reforming processes: carbon dioxide reforming, steam reforming, and partial oxidation reforming [27–29].

Nikoo and Amin [30] reported the main possible $CH_4$ and $CO_2$ reactions including those for the intermediate products such as ethane, ethylene, methanol, and dimethyl

Table 1: Composition of biogas derived from different feedstocks [3].

| Ref. | Biogas source | $CH_4$ (%) | $CO_2$ (%) | $N_2$ (%) | $O_2$ %) | $H_2S$ (%) | Other |
|---|---|---|---|---|---|---|---|
| Chen et al. [4] | Agricultural gases, landfill gas (LFG) | 45-75 | 25-55 | 0-25 | 0.01-5 | Trace | Trace composites (e.g., $NH_3$) |
| Vita et al. [5] | Biogas from a variety of organic raw materials | 50-75 | 25-45 | 2 | Trace | <1 | $H_2O$: 2-7% at 20-40°C<br>$H_2$: <1%<br>Trace composites (e.g., $NH_3$, siloxane, and halides) |
| Yentekakis et al. [6] | Biogas from digestion or anaerobic fermentation of most waste materials | 50-70 | 25-50 | — | — | — | — |
| Zhang et al. [7] | Biogas from urban organic waste | 40-70 | 30-60 | — | — | — | — |
| Broun and Sattler [8] | Biogas from solid waste in landfill | 45-60 | 40-55 | — | — | — | — |
| del Valle-Zermeño et al. [9] | Biogas from organic fraction of municipal solid waste | 55-70 | 30-45 | — | — | — | Some trace other gases |
| Díez-Ramírez et al. [10] Fei et al. [11] | LFG | 25-60 | 7-60 | — | 0.6-3 | — | $H_2O$: 3-20%<br>Trace amounts of other gases |
| Vita et al. [12] | Biogas from biomasses | 55-70 | 27-44 | — | — | <3 | $H_2$: <1%<br>Traces of siloxanes, $NH_3$, and halogenates |

Table 2: The main reaction equations involved in the process of DRM [18].

| Reaction equation | Standard reaction enthalpy | Reaction explanation |
|---|---|---|
| $CH_4 + CO_2 \rightleftarrows 2CO + 2H_2$ | $\Delta H_{298K} = 260.5$ kJ/mol | $CO_2$ reforming of methane (1) |
| $CO_2 + H_2 \rightleftarrows CO + H_2O$ | $\Delta H_{298K} = 41.0$ kJ/mol | Reverse water-gas shift (RWGS) (2) |
| $CH_4 + H_2O \rightleftarrows CO + 3H_2$ | $\Delta H_{298K} = 206.0$ kJ/mol | Steam reforming of methane (3) |
| $CH_4 + 2H_2O \rightleftarrows CO_2 + 4H_2$ | $\Delta H_{298K} = 165$ kJ/mol | Steam reforming of methane (4) |
| $CH_4 + 2O_2 \rightleftarrows CO_2 + 2H_2O$ | $\Delta H_{298K} = -802$ kJ/mol | Combustion of methane (5) |
| $CH_4 + 0.5O_2 \rightleftarrows CO + 2H_2$ | $\Delta H_{298K} = -36$ kJ/mol | Partial oxidation of methane (6) |
| $CH_4 \rightleftarrows C + 2H_2$ | $\Delta H_{298K} = 75.0$ kJ/mol | Decomposition of methane (7) |
| $2CO \rightleftarrows CO_2 + C$ | $\Delta H_{298K} = -172.5$ kJ/mol | Boudouard reaction (8) |
| $CO + H_2 \rightleftarrows H_2O + C$ | $\Delta H_{298K} = -131.5$ kJ/mol | CO reduction (9) |

ether (DME) and their corresponding equilibrium constants for a temperature range between 300 and 1200°C (see Table 3 and Figure 2).

Table 3 shows a more detailed list of possible DRM reactions compared to Table 2. In addition to the main reactions, it has been extended to include the reactions of the most important intermediate products as well. Alkanes and alkenes have often been reported as side products in DRM reactions. For instance, reactions 3 and 4 are the two main schemes for $CO_2$ oxidative coupling of methane to produce $C_2$ hydrocarbons. Ethane ($C_2H_6$) and ethylene ($C_2H_4$) are also potential intermediate products of methane decomposition (reaction 8), according to the suggested stepwise dehydrogenation mechanism [32, 33]. Further decomposition of ethylene can result in the appearance of acetylene ($C_2H_2$). However, this reaction is not listed by Nikoo et al. for the temperature range studied (between 300 and 1200°C).

Reactions leading to methanol and dimethyl ether were also considered in the study by Nikoo and Amin [30], although they are favored at lower temperatures than those typically used for DRM. Methanol can be produced by hydrogenation of CO and $CO_2$ (reactions 6 and 7), while it is consumed to form DME in reaction 15. $CO_2$ reforming and steam reforming of DME (reactions 12, 13, and 14) are active within the whole investigated temperature range (300-1200°C).

The equilibrium constants of all expected reactions are plotted versus temperature in Figure 2. A reaction is spontaneous if the change in the Gibbs free energy ($\Delta G_r$) is negative, based on the principles of thermodynamics. Inversely,

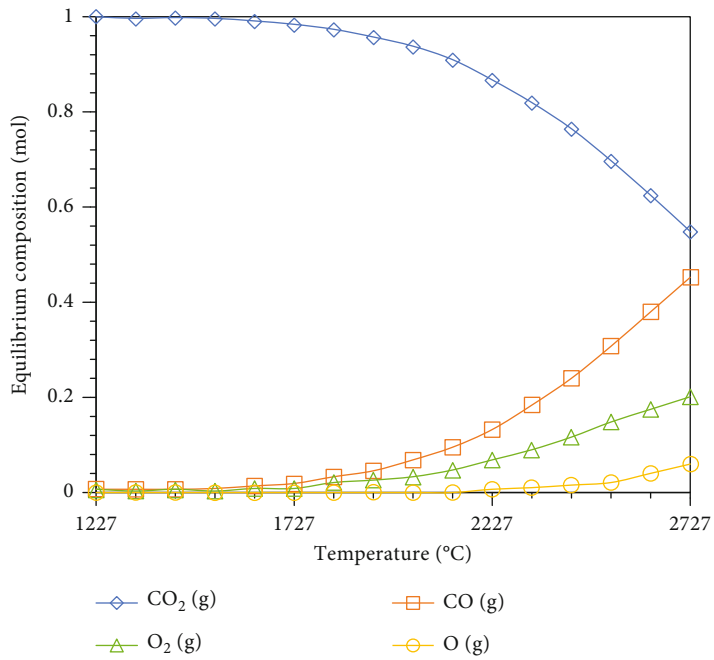


Figure 1: Equilibrium composition as a function of the temperature for 1 mol of $CO_2$ at 1 bar. Adapted from [24] with permission from ACS Publications. Copyright © 2008, American Chemical Society.

Table 3: Reactions involved in $CO_2$ reforming of methane according to Nikoo et al. [30] and cited by Aramouni et al. [31].

| No. | Reaction equation | $\Delta H_{298K}$ (kJ/Mol) | LnK at 300°C | LnK at 1100°C | Reaction explanation |
|---|---|---|---|---|---|
| 1 | $CH_4 + CO_2 \rightleftarrows 2CO + 2H_2$ | 247 | −20 | 13 | $CO_2$ reforming of methane |
| 2 | $CO_2 + H_2 \rightleftarrows CO + H_2O$ | 41 | -5 | 2 | Reverse water-gas shift |
| 3 | $2CH_4 + CO_2 \rightleftarrows C_2H_6 + CO + H_2O$ | 106 | -19 | -5 | $CO_2$ oxidative coupling of methane (formation of ethane) |
| 4 | $2CH_4 + 2CO_2 \rightleftarrows C_2H_4 + 2CO + 2H_2O$ | 284 | -36 | 0 | $CO_2$ oxidative coupling of methane (formation of ethylene) |
| 5 | $C_2H_6 \rightleftarrows C_2H_4 + H_2$ | 136 | -14 | 4 | Dehydrogenation of ethane |
| 6 | $CO + 2H_2 \rightleftarrows CH_3OH$ | -90.6 | -10 | -20 | Hydrogenation of CO |
| 7 | $CO_2 + 3H_2 \rightleftarrows CH_3OH + H_2O$ | -49.1 | -12 | -20 | Hydrogenation of $CO_2$ |
| 8 | $CH_4 \rightleftarrows C + 2H_2$ | 74.9 | -6 | 5 | Methane cracking |
| 9 | $2CO \rightleftarrows CO_2 + C$ | -172.4 | 15 | -7 | Boudouard reaction |
| 10 | $CO_2 + 2H_2 \rightleftarrows C + 2H_2O$ | -90 | 8 | -5 | $CO_2$ reduction |
| 11 | $H_2 + CO \rightleftarrows H_2O + C$ | -131.3 | 12 | -6 | CO reduction |
| 12 | $CH_3OCH_3 + CO_2 \rightleftarrows 3CO + 3H_2$ | 258.4 | 10 | 40 | $CO_2$ reforming of DME |
| 13 | $3H_2O + CH_3OCH_3 \rightleftarrows 2CO_2 + 6H_2$ | 136 | 20 | 37 | Steam reforming of DME |
| 14 | $CH_3OCH_3 + H_2O \rightleftarrows 2CO + 4H_2$ | 204.8 | 14 | 37 | Steam reforming of DME |
| 15 | $2CH_3OH \rightleftarrows CH_3OCH_3 + H_2O$ | -37 | 3 | -1 | Dehydration of methanol to DME |
| 16 | $CO_2 + 4H_2 \rightleftarrows CH_4 + 2H_2O$ | -165 | 14 | -10 | Methanation |
| 17 | $CO + 3H_2 \rightleftarrows CH_4 + H_2O$ | -206.2 | 14 | -11 | Methanation |

a positive $\Delta G_r$ means that the reaction is thermodynamically constrained. The equilibrium constant (K) dictates the maximum extent of a reaction. If K is much greater than 1, it is not possible to shift a reaction to the opposite side by modifying the molar ratio of the reactants. However, when K is close to 1, changing the molar ratio of the reactants significantly affects the product distribution. For any $\Delta G_r$ below 0, a larger value of LnK means that a spontaneous reaction is more favorable.

DRM is usually performed at temperatures in the range 650-1000°C [34]. From Figure 2, the following can be deduced:

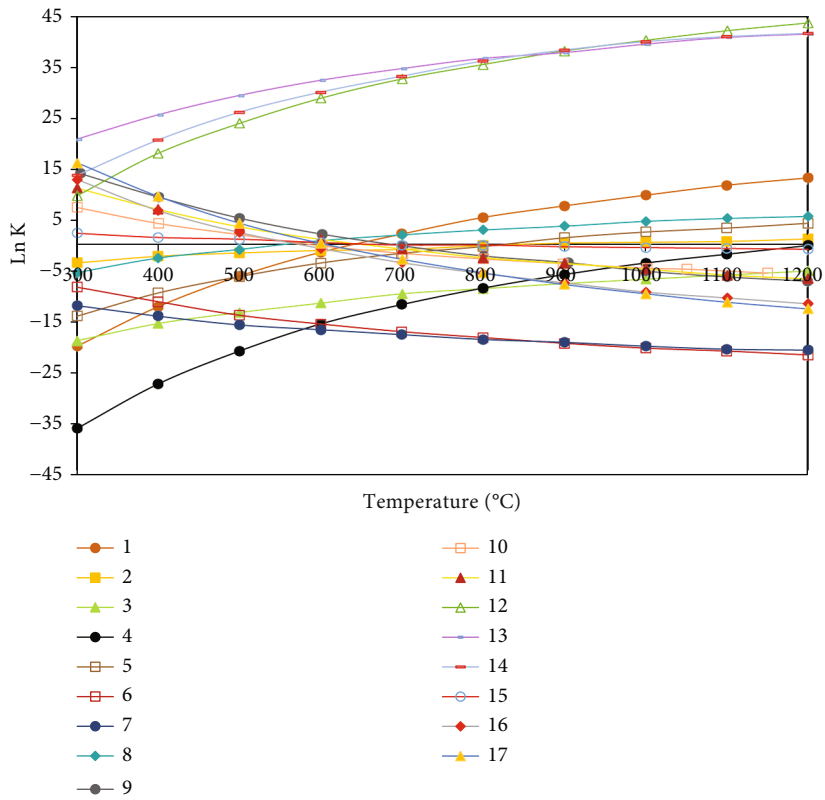


Figure 2: Equilibrium constants of the reactions involved in the $CO_2$ reforming of methane—given in Table 3 in matching order—at a temperature range between 300 and 1200°C. Reprinted with permission from [30]. Copyright © 2023 Elsevier B.V.

(i) The direct reaction of $CO_2$ and $CH_4$ to form syngas (reaction 1), the key reaction in DRM, is favored in particular at temperatures above 727°C [35]. Usually, $CO_2$ reforming of methane is accompanied simultaneously by the reverse water-gas shift (RWGS) reaction (number 2) [36], occurring more readily at higher temperatures

(ii) The formation of carbon at high temperatures is most likely to be caused by the decomposition of methane (reaction 8). Other reactions in which carbon is produced, the Boudouard reaction and the CO and $CO_2$ reductions (reactions 9, 10, and 11, respectively), are unlikely to occur at temperatures above 700°C, although they may be affected by equilibrium limitations at higher temperatures [19]

(iii) Reactions leading to ethane and ethylene formation (reactions 3 and 4, respectively) are only possible at elevated temperatures [37] (due to the high negative values of Ln(K) for the temperature range studied). The dehydrogenation of ethane to ethylene (reaction 5) takes places in parallel with reactions 3 and 4. While it can also be limited by equilibrium, increasing the temperature promotes its occurrence

(iv) In the case of $CO_2$ and CO hydrogenation (reactions 6 and 7, respectively), their reverse reactions are strongly favored at high temperatures [38] as indicated by their negative Ln(K) values

(v) Increasing the temperature in the considered range can promote the progression of reactions 12, 13, and 14 towards the right-hand side. On the other hand, reaction 15 is highly susceptible to equilibrium limitations as it has Ln(K) values close to zero

(vi) Methanation reactions 16 and 17 are limited at high temperatures due to their exothermic nature and negative Ln(K) values [39].

In their study, Nikoo and Amin [30] also investigated the effect of $O_2$ addition on the reforming of methane with $CO_2$. They observed that an increase in $O_2$ content resulted in higher $CH_4$ conversion rates and a smaller risk of carbon formation at lower temperatures. Conversely, $O_2$ was observed to significantly decrease $CO_2$ conversion rates and CO and $H_2$ yields, but resulted in an increase in water formation.

The thermodynamic equilibrium conversions of $CH_4$ and $CO_2$ for a $CH_4:CO_2$ ratio of 1 in the feed are shown in Figure 3. Özkara-Aydınoğlu [40] performed these calculations at equilibrium by total Gibbs free energy minimization of the dry-reforming system for a temperature range of 200-1400°C and at three different pressures (1, 10, and 20 bar).

At 1 bar, $CH_4$ conversion (Figure 3(a)) starts from 350°C and reaches almost 100% conversion by 900°C [41]. $CO_2$ conversions (Figure 3(b)) are higher than the corresponding

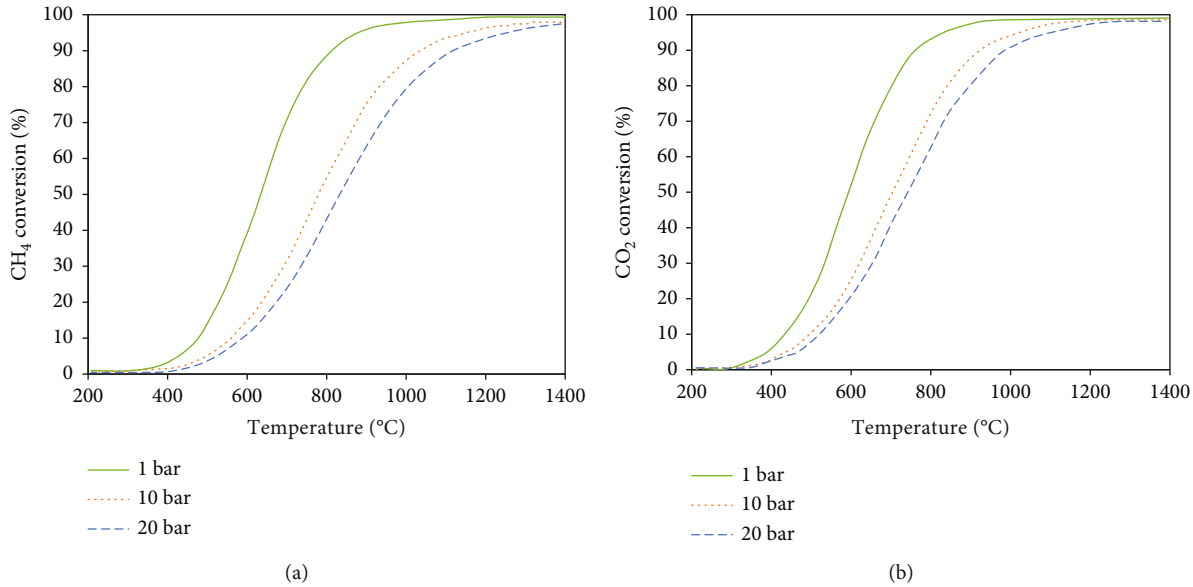


Figure 3: Conversion of $CH_4$ (a) and $CO_2$ (b) for dry reforming with $CH_4 : CO_2 = 1$ calculated for the temperature range 200–1400°C at 1, 10, and 20 bar. Adapted with permission from Ref. [40]. Copyright © 2023 Professor T. Nejat Veziroglu.

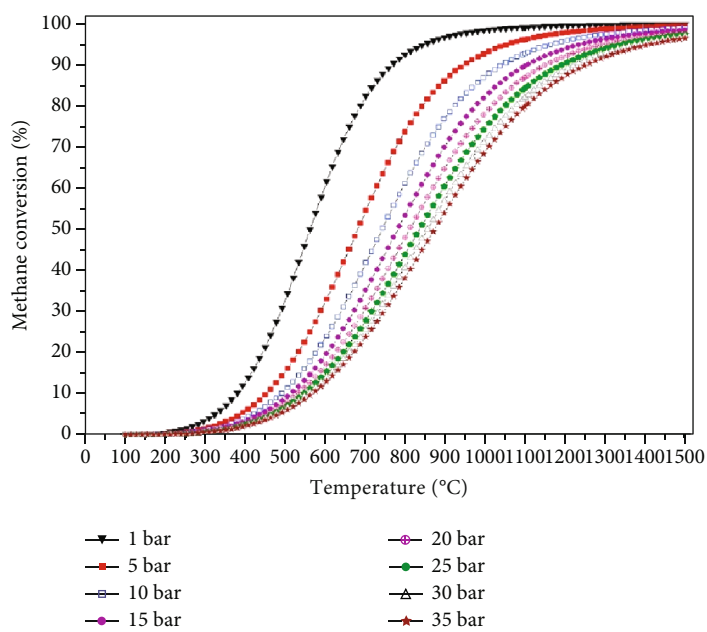


Figure 4: Equilibrium methane conversions of methane pyrolysis for temperatures up to 1500°C and pressures from 1 bar to 35 bar. Reprinted with permission from Reference [42].

$CH_4$ conversions as a consequence of the reverse water-gas shift equilibrium.

Higher pressures negatively impact DRM, following a similar trend to methane pyrolysis (see Figure 4). The conversions obtained, both for $CH_4$ and for $CO_2$, exhibit a notable decrease with increasing pressure. However, the effect of pressure is almost negligible when the temperature is below 400°C or above 1200°C.

It was also found that the formation of carbon and water increases with increasing pressure [43]. The syngas $H_2$/CO ratio decreases at higher operation pressures [40], although an elevated temperature suppresses the effect of pressure.

In addition, the equilibrium shifts significantly depending on the $CO_2$ content of the biogas used as feedstock. Figure 5 shows the influence of the molar ratio of $CH_4$/$CO_2$ on the thermodynamic equilibrium of a biogas mixture.

For example, a reactant mixture with 50% of $CO_2$ (Figure 5(a)) produces a syngas with a $H_2$/CO ratio of around 1 at a reaction temperature of 1000°C, while for lower $CO_2$ content in the educt gas mixture, the $H_2$/CO ratio

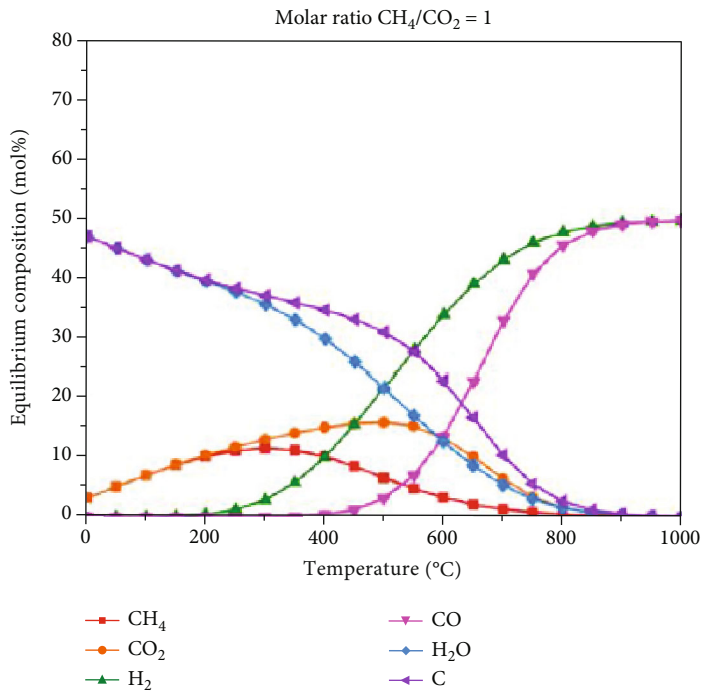


(a)

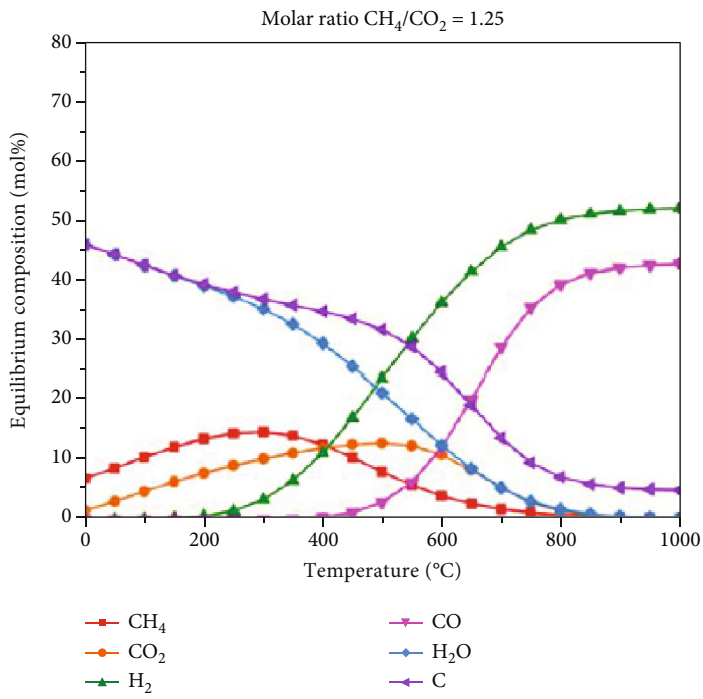


(b)

Figure 5: Continued.

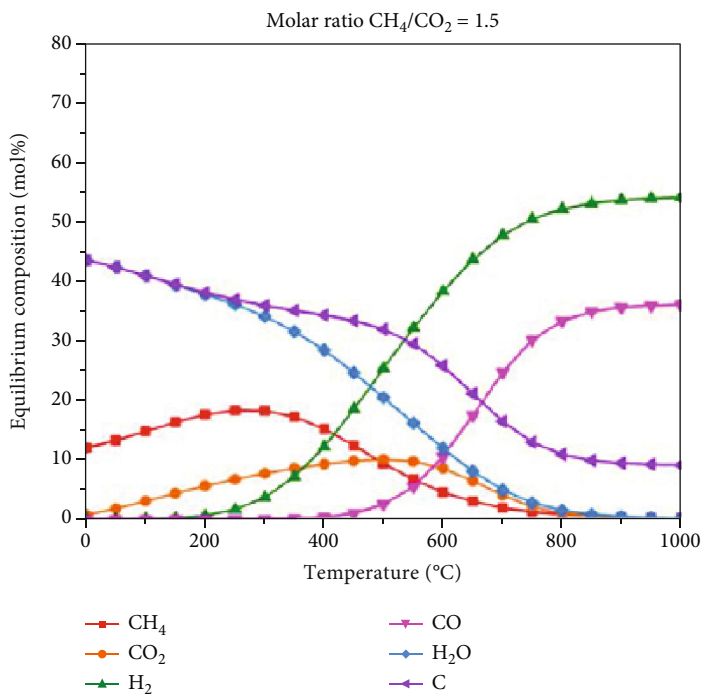


(c)

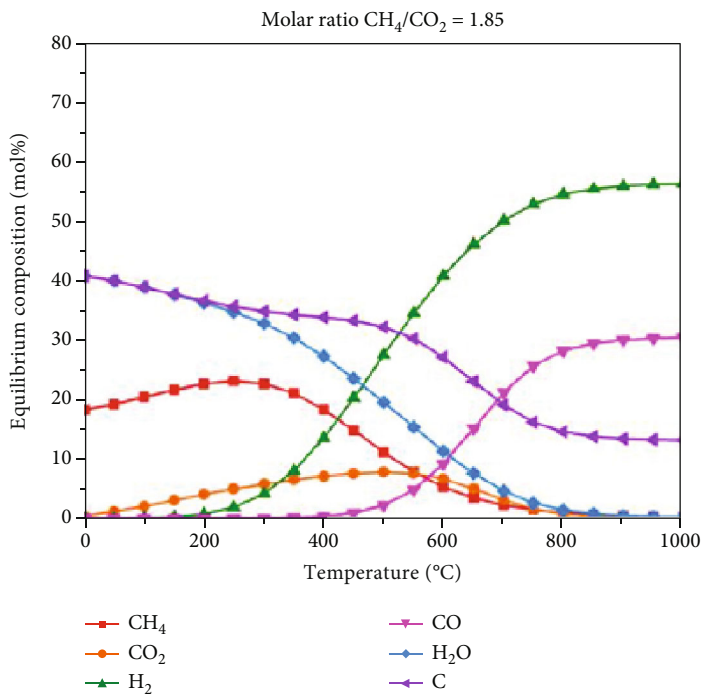


(d)

Figure 5: Thermodynamic equilibrium plots of DRM under different biogas mixtures at 1 bar. Reprinted with permission from [44]. Copyright © 2021 le Saché, Alvarez Moreno, and Reina.

of the product increases significantly. Also, a higher tendency towards carbon deposition can be observed for higher $CH_4/CO_2$ ratios in the feed gas. Therefore, the molar ratio $CH_4/CO_2$ in the biogas greatly influences the $H_2/CO$ molar ratio in the syngas product.

Although $C_2H_2$ was not included in the thermodynamic analyses of DRM previously mentioned [30, 44], it is an important intermediate product of methane pyrolysis [32]. Therefore, we performed an analysis of the thermodynamic equilibrium compositions for a temperature range from

300 to 1200°C and initial ratios of $CH_4/CO_2$ of 0.5, 1, and 2 using the software AspenPlus and an RGibbs reactor model. Figure 6 shows the thermodynamic equilibrium results obtained for the following possible intermediate products: $CH_2O$, $CH_3OH$, $C_2H_6$, $C_2H_4$, and $C_2H_2$. It shows that, for instance, for an initial $CH_4/CO_2$ ratio of 1 : 1 (Figure 6(b)), at temperatures above 1050°C, more $C_2H_2$ than $C_2H_6$ is expected at the thermodynamic equilibrium. Consequently, based on our analysis, it is crucial to consider $C_2H_2$ as a potential by-product of DRM, in addition to the products mentioned by Nikoo and Amin [30].

*1.2.2. Kinetics of Dry Reforming of Methane.* While the thermodynamics of the dry-reforming reaction are fairly understood, the mechanism and kinetics are less known. In addition, both will be modified if a catalyst is introduced to reduce the activation energy required for the process and to favor the selectivity towards syngas production [45]. Catalysts usually employed in DRM are transition metals (Ni, Co, and Fe) or noble metals (Pd, Rh, Ru, Pt, and Ir) [46, 47]. In particular, Ni is the most widely studied base metal for this reaction due to the high activity, low cost, and higher commercial feasibility [48].

Since a major problem associated with DRM is the deposition of carbon on the catalytic system, leading to its deactivation, great efforts are being made to solve this problem. Some strategies include adding oxygen and/or steam in the feed [49] or operating at reaction conditions where carbon formation is thermodynamically restrained [50].

Several studies have attempted to solve the problem by developing catalysts [31, 51–53]. Common catalyst modifications reported to limit coking are for example the addition of promoters [54, 55], the use of a bimetallic system [56, 57], doping with rare earth metals [58], supporting on refractory oxides [59], or the introduction of a single site catalyst [60]. Usman et al. [61] investigated the influence of several process parameters on catalytic activity, stability, and carbon deposition in order to suggest future research. An alternative procedure proposed by Kumar [62] consists of adding ammonia to the feed. The results show that ammonia not only contributes to the suppression of carbon formation (although a complete carbon-free product can only be achieved with a molar ratio $NH_3/CH_4 \geq 4$) but also significantly increases hydrogen production.

To overcome the limitations of traditional catalysts, Kodama et al. evaluated methane dry reforming in a bubble reaction system containing a metal catalyst powder dispersed in a molten salt mixture [63, 64]. Only few publications have been found in which dry reforming of methane has been carried out in bubble column reactors filled with molten salts [63, 65] or liquid metals ($Ni_{0.65}In_{0.35}$ [17]) or a system with both ($Ni_{0.27}Bi_{0.73}$–$K_2CO_3$ [66]). The results of the latter two studies carried out with liquid metals are discussed later in this work.

*1.3. Molten Media Reactor for Chemical Processes.* Molten salts and liquid metals (LM) are excellent heat transfer fluids, as can be seen in Table 4, which make them particularly suitable for deployment in high temperature chemical processes.

Most liquid metals have a lower melting point than molten salts and a higher boiling point, offering a larger operating temperature range, especially the so-called fusible metals (like Ga, In, Sn, and Bi) [71]. They also usually present higher thermal conductivity, lower viscosity, and lower heat capacities compared to salts.

The use of LM has already been proposed for methane cracking as it presents significant advantages for heat transfer and at the same time supports carbon separation, since the solid carbon floats on the liquid metal surface due to the metal's higher density and can thus be removed. Investigations have been conducted with different liquid metals such as Sn [72–74], Ga [42], or alloys NiBi [75] and CuBi [76]. Certain types of molten salts that are stable at high temperatures are another promising reaction media for the production of fuels. They have been previously used for biomass gasification [77] and pyrolysis of methane [78–83].

A limited number of studies in literature have evaluated the possibility of employing molten salts and/or liquid metals for the dry reforming of methane. The thermodynamic properties of different metal candidates are summarized in the diagram in Figure 7.

As a conclusion, based on thermodynamic and practical constraints, Fe, Sn, In, Ga, and Mn were identified as the most promising candidates. Therefore, tin satisfies the three criteria: Sn does not form a stable carbide, it can be oxidized by $CO_2$, and Sn oxides can be reduced by $CH_4$.

Consequently, a bubble reactor filled with liquid tin presents a potential application for conducting the DRM, thus avoiding the currently existing challenges of catalyst deactivation by carbon deposition [53]. Although Sn has not yet been studied for DRM, the suitability of tin as a heat transfer medium for methane pyrolysis has been demonstrated in a LM bubble column reactor.

Since 2012, the Karlsruhe Liquid Metal Laboratory (KALLA) at the Karlsruhe Institute of Technology (KIT) has been working on an innovative approach to hydrogen production via methane pyrolysis using liquid metal technology, developed in collaboration with the Institute for Advanced Sustainability Studies [73, 84]. The choice of Sn as the working fluid was driven by multiple factors, including its relatively low melting point, nontoxic and nonexplosive nature, good thermal conductivity, and high density compared to carbon. Furthermore, Sn exhibits long-term chemical stability and is inert towards the reaction gases and carbon [67]. Its relatively lower cost compared to other liquid metals was another advantage. However, the use of liquid tin is not without its challenges, as it can cause strong corrosion attack towards metallic materials, especially steel, at high temperatures [84].

In a laboratory set-up, a series of experimental runs were conducted using a 1.3 m high reactor with a 4 cm inner diameter, containing liquid tin filled up to a level of 1 m during operation. The methane feed gas was introduced into the reactor through a single orifice (Ø = 0.5 mm) at the bottom, while the resulting gas was discharged from the top. All parts of the reactor in contact with liquid tin are made of quartz glass, which has proven to be chemically resistant against tin corrosion and stable in operating conditions up to

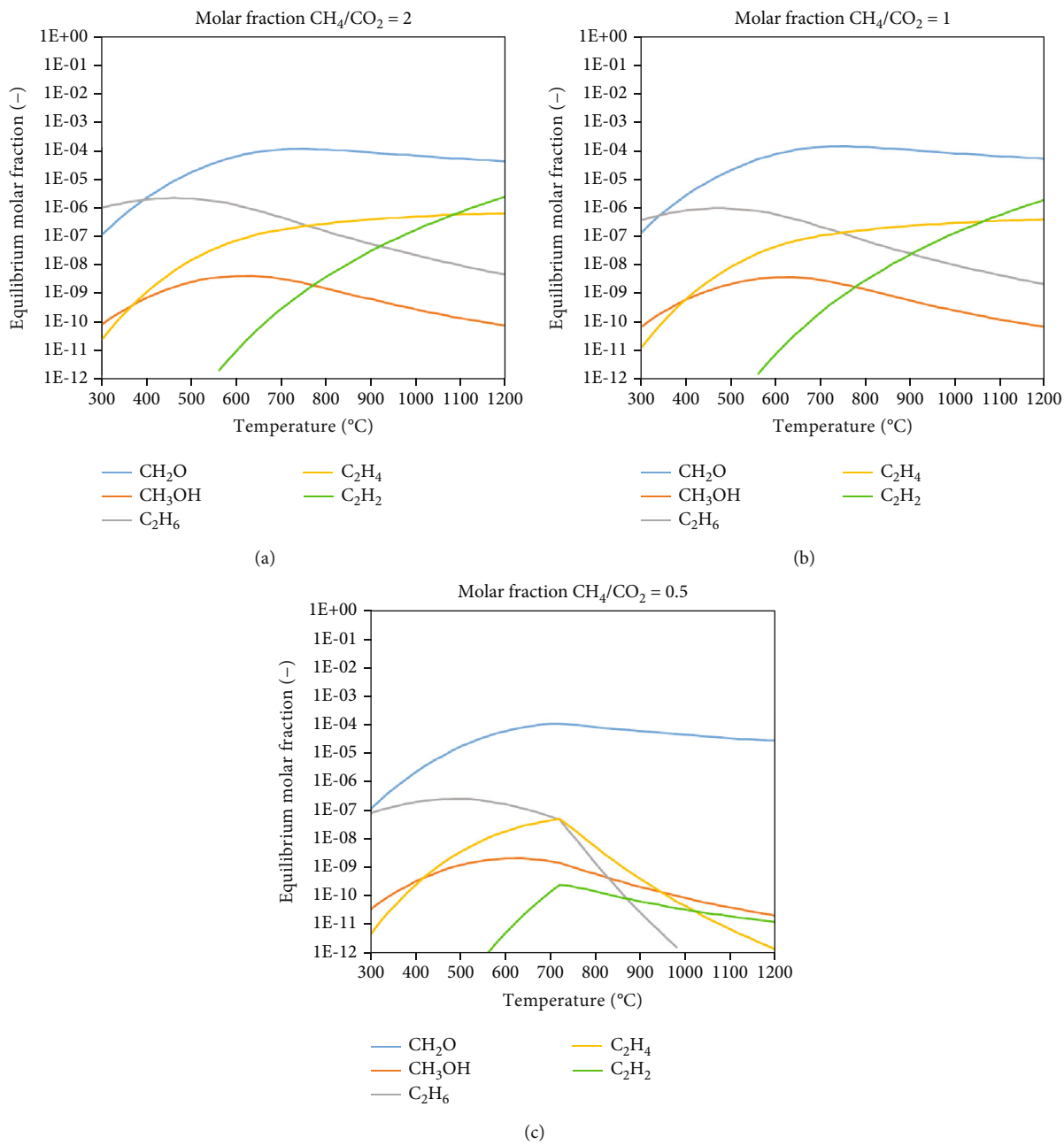


Figure 6: Thermodynamic equilibrium results of DRM obtained for $CH_2O$, $CH_3OH$, $C_2H_6$, $C_2H_4$, and $C_2H_2$ at 1 bar under different biogas mixtures: (a) $CH_4/CO_2 = 2$, (b) $CH_4/CO_2 = 1$, and (c) $CH_4/CO_2 = 0.5$.

1200°C. A methane conversion of 78% was obtained in the previously described set-up by Geißler et al. at 1175°C and atmospheric pressure [85].

The experience gained in the use of this type of reactor will be useful for its application in the dry reforming of biogas. Having reviewed the characteristics of biogas and the challenges of dry reforming as a means of converting biogas into synthesis gas, it is important to highlight how the proposed solution seeks to fill an existing gap in this area of research. Most current research focuses on developing new catalysts or optimizing conditions to avoid carbon formation during DRM. However, this may not always be possible in the case of biogas, since $CH_4$ content is usually higher than that of $CO_2$, and an excessive amount of methane contributes significantly to carbon formation.

A first step in applying this technology is then performed in the following Section 2 by presenting the authors' own contribution with a theoretical study on the by-products formed during the dry reforming of biogas while specifically using a reactor filled with liquid tin. This chapter includes a detailed discussion of the formation of carbon, water vapor, and the possible presence of tin carbides and tin oxides. By providing a comprehensive analysis of these compounds, this study is aimed at advancing the understanding of dry biogas reforming and paving the way for future experimental research in this field.

Table 4: Thermophysical properties of heat transfer fluids.

| | | $T_{min}$ (°C) | $T_{max}$ (°C) | $c_p$ (kJ/kg K) | $\lambda$ (W/mK) | $\rho$ (kg/m$^3$) | $\mu$ (mPa/s) | Ref. |
|---|---|---|---|---|---|---|---|---|
| Air | | — | — | 1.12 | 0.06 | 0.40 | 0.03 | [67] |
| Water/steam | | 0 | — | 2.42 | 0.08 | 22.1 | 0.03 | [67] |
| Molten salts | Solar salt | 220 | 600 | 1.10 | 0.52 | 1903 | 1.33 | [67] |
| | $K_2CO_3$ | 897 | — | — | — | 2290 | — | [68] |
| | $Na_2CO_3$-$K_2CO_3$ (49-51 wt%) | 710 | — | 1.56 | 1.73 | — | — | [69] |
| | $ZnCl_2$-NaCl-KCl (68.6-7.5-23.9 wt%) | 204 | 850 | 0.9 | 0.29 | 1977 | 4.2 | [70] |
| | KCl-$MgCl_2$ (62.5-37.5 wt%) | 426 | 800 | 1.15 | 0.5 | 1660 | 5.0 | [70] |
| Liquid metals | Sn | 232 | 2687 | 0.24 | 33.8 | 6330 | 1.01 | [67] |
| | Bi | 271 | 1670 | 0.15 | 16.3 | 9940 | 1.17 | [67] |
| | In | 157 | 2072 | 0.24 | 47.2 | 6670 | 0.75 | [67] |
| | Ga | 30 | 2237 | 0.36 | 50.0 | 6090 | 0.77 | [67] |
| | Pb | 327 | 1743 | 0.15 | 18.8 | 10324 | 1.55 | [67] |
| | PbBi eutectic (44.5-55.5 wt%) | 125 | 1533 | 0.15 | 12.8 | 9660 | 1.08 | [67] |

$\Delta T$: liquid temperature range; $c_p$: specific heat capacity; $\lambda$: thermal conductivity; $\rho$: density; $\mu$: dynamic viscosity. Ref. [67] properties at 600°C and 1 bar; in Refs. [68, 69], measurement temperature not specified; Ref. [70] at 700°C.

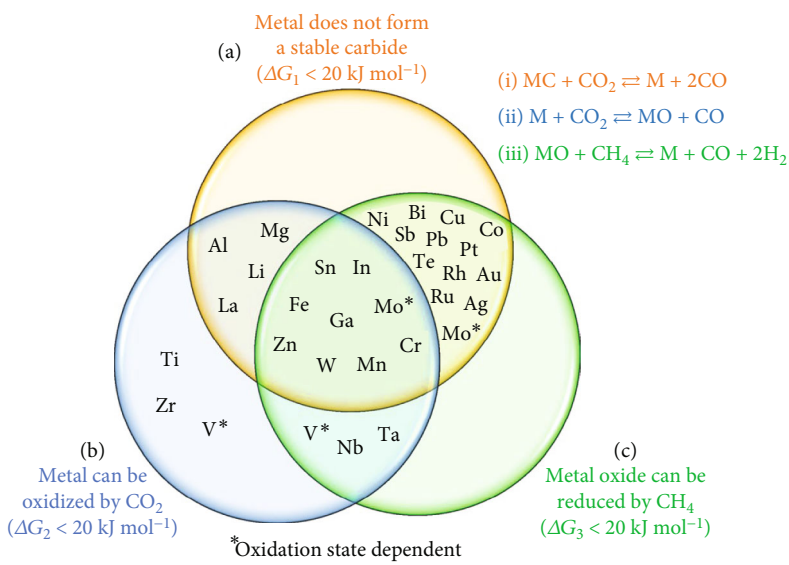


Figure 7: Summary of thermodynamic properties of eligible metal candidates for participation in a $CH_4/CO_2$ redox cycle for DRM. Criteria include the following: a—the metal carbide is unstable, b—the metal can be oxidized by $CO_2$ to all of the possible oxidation states, and c—all of the possible metal oxides can be reduced by $CH_4$. Each thermodynamic criterion is met if the corresponding $\Delta G_r$ is less than +20 kJ mol$^{-1}$ at 1080°C. Reprinted with permission from [17]. Copyright © 2020, Clarke Palmer et al., under exclusive licence to Springer Nature Limited.

Afterwards, in Section 3, we discuss the practical implementation supported by the limited available results found for DRM in molten media. All this information is used to draw our own conclusions about the feasibility of using a reactor filled with liquid tin.

A specific feature of the proposed technology is that the liquid metal used in the reactor is an intermediate energy transmitter from the heat source to the initial reactants of the chemical process. Due to the high thermal conductivity of the liquid metal, it is possible to transfer heat intensively to each gas bubble dispersed in the reactor, thus achieving a larger heat exchange surface compared to alternative processes. The liquid metal does not leave the bubble reactor and is not recirculated, so only an initial one-time heating of the liquid metal to the required temperature level is necessary. Furthermore, in the process itself, only the heat losses required to heat the initial gas mixture to the reaction temperature and the heat losses of the furnace used need to be compensated.

It should be noted that for a favorable energy balance in the future industrial plant, heat energy recovery must be realized. This can be achieved by preheating the initial reagents by the reaction products leaving the reactor. A specific quantitative evaluation of the energy consumption and, in general, of the cost of the process, in relation to the heat losses of the furnace used and the efficiency of the energy

recovery system, is possible only after reaching a higher level of technological development and analyzing the results of the practical operation of the pilot plant.

## 2. Theoretical Study: Possible Compounds Formed in Biogas Dry Reforming Using a Reactor Filled with Liquid Tin

During the DRM process, several reactions take place simultaneously depending on the operating temperature, pressure, and varying feed compositions. In the following, we evaluate the different components formed and reactions that would theoretically take place using a bubble column reactor filled with a liquid metal (Sn), without the addition of any other catalyst, operating at high temperatures of around 1000°C and atmospheric pressure. Therefore, in addition to the reactions of the DRM process itself, the possible reactions that could take place with the tin are analyzed. Below, the formation of carbon and water vapor, as well as the potential presence of tin compounds such as carbides or oxides, is discussed in more detail.

*2.1. Carbon Formation.* Carbon formation in dry reforming may occur via decomposition of methane or disproportionation of carbon monoxide (Boudouard reaction). Between 550 and 700°C, the Boudouard reaction is particularly pronounced, and above 900°C, methane pyrolysis [17]. Other possible reactions in which carbon may be formed are the hydrogenation of carbon dioxide and carbon monoxide, in which carbon tends to be formed at lower temperatures (<527°C).

All reactions involved in carbon formation can be affected by operating parameters due to their low equilibrium constants [30]. Carbon is found to be formed in the entire range of temperature at $CO_2/CH_4$ feed ratio < 1 [37, 47]. The range of conditions under which carbon forms in the equilibrium system is depicted in Figure 8. Carbon formation decreases with increasing temperature and higher $CO_2/CH_4$ feed ratio (>1).

For the thermodynamic equilibrium at temperatures above 700°C and atmospheric pressure, a smaller amount of carbon is expected to be formed than in the pyrolysis of pure methane [86]. This is due to the Boudouard reaction, which runs in parallel with pyrolysis and whose equilibrium at a temperature > 700°C is on the CO side with carbon and $CO_2$ consumption, as can be seen in Figure 2.

Some differences in the solid carbon produced by using biogas as educt compared to feeding pure methane into the pyrolysis reactor are likely. The pyrolytic carbon collected from above the tin surface by Geißler et al. [85] appeared in powder form with particle sizes in the range of 15–20 $\mu$m. Upham et al. [75] reported loose graphitic powder, which they collected from the surface of a 27 : 73 mol% Ni : Bi alloy after hours of methane pyrolysis. The characterization carried out by Palmer et al. [17] of the carbon product collected from the surface of the 65 : 35 mol% Ni : In alloy after hours of combined dry reforming and methane pyrolysis showed that it had microscale polycrystalline structures, specifically identified as nanocrystalline graphite. Both carbon samples were analyzed by Raman spectroscopy showing distinctive D and G peaks. The D band (~1350 $cm^{-1}$) indicates the presence of defects in the graphitic lattice, and the G band (~1580 $cm^{-1}$) corresponds to sp2 hybridized graphitic carbon [87]. Highly graphitic carbon is more resistant to oxidation and gasification than less ordered carbon morphologies. The ratio of the D and G band intensities (ID/IG) was 0.584 for the pyrolytic carbon [75] and 3.24 for the DRM carbon product [17]. According to Palmer et al. [17], it is likely that the carbon species that are converted to CO through the reverse Boudouard reaction are intermediate and/or amorphous carbons formed from the decomposition of methane. They also stated that, in contrast, graphitic species accumulate on the surface of the bubble column.

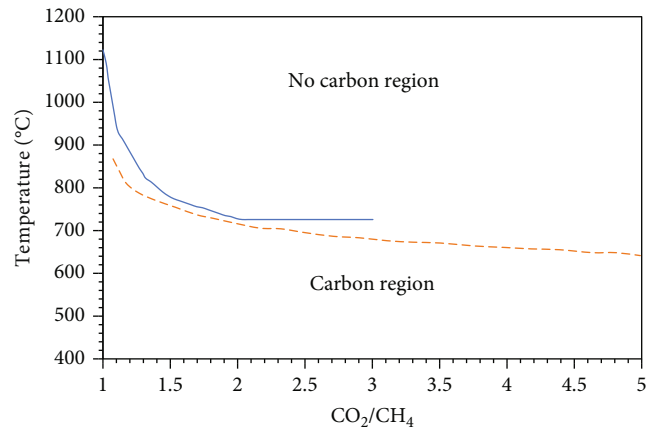


Figure 8: Carbon and no carbon formation regions at 1 atm as a function of temperature and the $CO_2/CH_4$ feed ratio. Data from Ref. [37] (solid line) and Ref. [47] (dashed line).

While the ID/IG ratio of the Raman spectra reported by Upham et al. [75] and Palmer et al. [17] differ greatly, indicating significant discrepancies in the carbon products, the differences in the obtained carbon might have further causes in addition to the presence of $CO_2$. The composition of the LM alloys in the two studies differs, as well as the partial pressure of methane. Although there is not much literature on the effect that different metal alloys have on the carbon produced by methane pyrolysis, different LM substrates, synthesis temperatures, residence times, and a variation of the hydrogen partial pressure resulted in significant changes in the quality and layer number of graphene obtained by chemical vapor deposition (CVD) from methane [88]. Without a more thorough experimental analysis to eliminate these differences in synthesis conditions, a definitive conclusion regarding the effect of $CO_2$ on the carbon product formed is not possible.

Indeed, solid carbon formation is a desired effect in view of using the DRM process as part of technologies that target $CO_2$ emission reduction or even such that intend to achieve negative emissions (NET). If such technology is combined with biological sources for the energy, like in biogas production, they are commonly referred to as BECCS (bioenergy carbon capture and storage) [89–91].

*2.2. Water Vapor.* The amount of water obtained in the final product will depend on the $CH_4/CO_2$ ratio of the biogas feed and the process temperature. Nikoo and Amin [30] plotted the equilibrium moles of water obtained as a function of temperature and the $CO_2/CH_4$ ratio (Figure 9).

Water formation follows a similar downward trend regardless of the $CO_2/CH_4$ ratio up to 700°C. However, at higher temperatures, two different trends are observed: at $CO_2/CH_4$ ratios of 2 and 3, the number of water moles reaches a minimum and then increases again with temperature, while at lower ratios, the water formed continues to decrease. These results are consistent with the conclusion of Palmer et al. [17] that for their reaction conditions ($CH_4/CO_2 = 2$, i.e., $CO_2/CH_4 = 0.5$), $H_2O$ is not present at thermodynamic equilibrium. Although $H_2O$ was produced in some of the reactions that took place (RWGS or the reduction of metal oxide with $H_2$), it was immediately consumed in either the steam gasification of solid carbon or steam methane reforming and was not obtained in the final product.

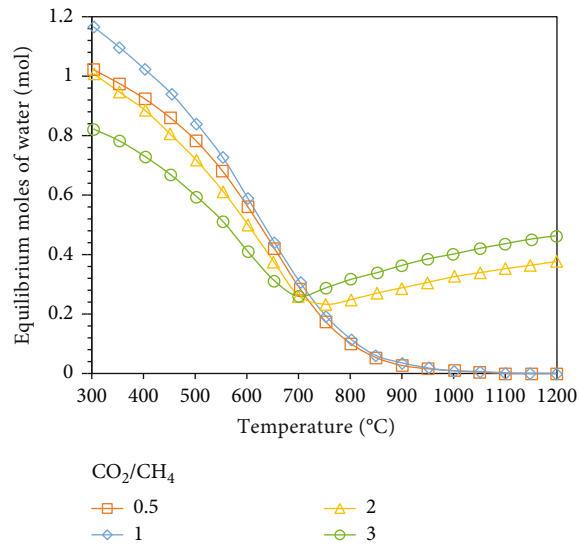


Figure 9: Moles of water as a function of temperature and $CO_2/CH_4$ ratio at 1 atm for $n(CH_4 + CO_2) = 2$ mol. Adapted with permission from Ref. [30]. Copyright © 2010 Elsevier B.V.

*2.3. Liquid Tin Reactor for Biogas Reforming.* When using a molten metal reactor, it is important to consider the various reactions that can occur with the metal depending on the operating temperature. First, the liquid metal itself must be considered because Sn could catalyze the reaction of $CO_2$ and C (Boudouard reaction) according to the work of Epstein et al. [92]. Their thermogravimetric analysis (TGA) experiments showed that the carbothermal reduction rate is much faster than the oxidation rate. Padilla and Sohn [93] also demonstrated the catalytic effect of tin on the Boudouard reaction by oxidizing coconut charcoal mixed with particles of tin.

$H_2$, $N_2$, Ar, He, CO, and $CO_2$ are practically insoluble in solid and liquid tin [94]. However, $CO_2$ oxidizes the liquid metal at above approximately 550°C. Furthermore, tin begins to react with water vapor at 650 to 700°C [94]. The oxidation of tin by water vapor proceeds according to this reaction:

$$Sn(s) + 2H_2O \longleftrightarrow SnO_2 + 2H_2 \quad (1)$$

Although tin could potentially react with the water vapor to produce hydrogen and tin oxide, the thermodynamics are unfavorable (see Table 5) and would require a long contact time [95].

*2.3.1. Tin Carbides.* Carbides are compounds originating from the reaction of carbon with another, less electronegative element. Commonly, this means a binary compound of carbon and a metallic element. The reaction of carbon with metals of "groups 1 and 2" and aluminum produces ionic carbides, whereas carbon forms interstitial carbides with most transition metals.

However, although many metals can easily form carbides, tin is reported to behave inertly toward carbon. According to different literature sources, Sn has no (or a very low) solubility for carbon and does not form carbides [96, 97]. This has been proven also in the long-term experiments at up to 1250°C in KALLA [85]. Noticeable carbon solubility is found at the boiling point (2600°C) [98]. According to the correlation of Oden and Gokcen [99], the solubility of carbon in molten tin is $2.23 \times 10^{-4}$ wt% at 1550°C and $1.01 \times 10^{-3}$ wt% at 1750°C. These values are in the order of magnitude of those found for other metals such as pure molten copper (about $4 \times 10^{-4}$ wt% at 1475°C [100] and $3 \times 10^{-3}$ wt% at 1700°C [101]). In comparison, the solubility of C in Ni in the liquid state reaches 5 wt% at 1750°C [100], while in Fe, it is about 20.5 wt% at 1550°C [102].

*2.3.2. Tin Oxides.* Tin can form two main oxide compounds: tin (II) oxide or stannous oxide with the formula SnO and tin dioxide ($SnO_2$), also known as stannic oxide. The formation of the lower oxide of tin, SnO, is thermodynamically unfavorable. Platteeuw and Meyer [103] showed experimentally that solid stannous oxide (SnO (s)) is unstable and decomposes into tin and tin dioxide at 300°C and higher, while gaseous stannous oxide (SnO (g)), on the other hand, is stable. Possibly, at least between 300 and 1127°C, $SnO_2$ (s) and SnO (g) are the only stable oxide phases [98].

Nevertheless, $SnO_2$ will be reduced by carbon at any temperature above 630°C as shown in Figure 10. Padilla and Sohn [93] investigated the rate of reduction of $SnO_2$ (stannic oxide) by carbonaceous materials in the temperature range 800 to 1000°C. The reduction of $SnO_2$ by carbon is usually represented by the following equation:

$$SnO_2(s) + C(s) \longleftrightarrow Sn(s, l) + CO_2(g) \quad (2)$$

However, consecutive reduction and oxidation reactions occur through the gaseous intermediates $CO_2$ and CO. The direct reaction between solid oxide and solid carbon is important only when the gaseous products of reaction, i.e., CO and $CO_2$, are removed from the reaction system.

Table 5: Thermodynamic data for tin oxidation reactions [95].

| Reaction | $\Delta H_r^\theta$ at STP (kJ mol$^{-1}$) | $\Delta S_r^\theta$ at STP (kJ mol$^{-1}$) | $\Delta G_r^\theta$ at STP (kJ mol$^{-1}$) |
|---|---|---|---|
| $Sn + 2H_2O \longrightarrow SnO_2 + 2H_2$ | -97 | -115.2 | -62.67 |
| $Sn + H_2O \longrightarrow SnO + H_2$ | -44 | -53 | -28.21 |

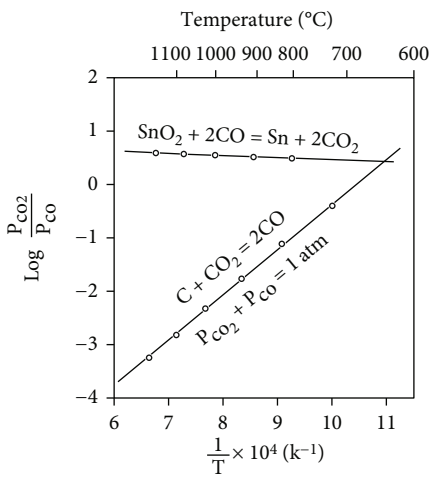


Figure 10: Theoretical equilibrium ratio $P_{CO2}/P_{CO}$ as a function of temperature for $SnO_2$ reduction. Reprinted with permission from [93]. Copyright © 1969, American Society for Metals and the Metallurgical Society of Aime.

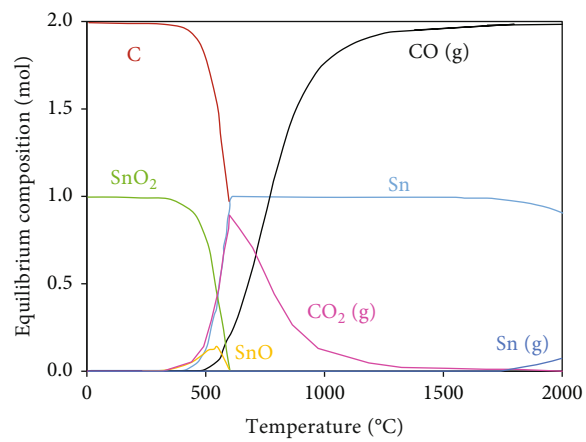


Figure 11: Equilibrium composition of the $SnO_2 + 2C$ system at 1 bar without inert gas dilution. Adapted with permission from [105]. Copyright © 2014, American Chemical Society.

Thus, the two-stage mechanism proceeds as follows:

$$\begin{aligned} SnO_2(s) + 2CO(g) &\longleftrightarrow Sn(s,l) + 2CO_2(g) \\ CO_2 + C(s) &\longleftrightarrow 2CO(g) \end{aligned} \quad (3)$$

The overall rate of reduction is controlled by the oxidation of carbon by $CO_2$. Temperature and the type of carbon greatly influence the reaction rate. An activation energy of 220.9 kJ/mol was calculated for the reduction of $SnO_2$ with coconut charcoal within the temperature range 800 to 900°C and 323.8 kJ/mol with graphite within the temperature range 925 to 1000°C [93].

The carbothermal reduction of $SnO_2$ has been extensively studied in several articles of Abanades and colleagues because of its possible application as part of a two-step thermochemical process for solar fuel production [23, 104–106]. In thermodynamic equilibrium at 1000°C, $SnO_2$ is completely reduced to metallic tin, and more than 85% of carbon is converted to CO as shown in Figure 11, which summarizes the equilibrium composition of a $SnO_2 + 2C$ mixture as a function of the temperature [105].

Ha et al. [107] theoretically investigated the $CH_4$-$SnO_2$ interaction at the atomic level and found that $CH_4$ provides a reducing atmosphere because the carbon and hydrogen of $CH_4$ sequentially reduce $SnO_2$ and produce various gas-phase products (see Figure 12).

The material-related aspects of the thermal decomposition of methane in liquid tin, including corrosion problems and the formation of carbides, have been studied by Emmerich [108]. A key requirement for choosing a suitable liquid metal is that it is thermally stable above 700°C and does not form carbides or hydrides, so that the reactor is not clogged by nonmetallic solids. These criteria are met in particular by the liquid metal tin [94, 98] which is why Sn was used in that work and in a parallel reactor development.

Considering these aspects presented, we come to the following conclusions regarding the suitability of a bubble column reactor filled with molten tin for DRM:

(i) Both carbon and water vapor formation are greatly influenced by temperature and the $CO_2/CH_4$ feed ratio

(ii) In biogas, the $CO_2/CH_4$ feed ratio typically falls between 0.5 and 1, as shown in Table 1. This ratio is beneficial as it leads to minimal water vapor production at high operating temperatures ($T > 1000$ °C), as depicted in Figure 8

(iii) However, for $CO_2/CH_4$ ratios < 1, carbon formation becomes inevitable if the thermodynamic equilibrium is reached, as demonstrated in Figure 7

(iv) These findings underscore the advantages of using bubble column reactors filled with liquid metals to facilitate the removal of the solid carbon. Tin is a good candidate since it does not form unwanted compounds with the reactants or products of DRM

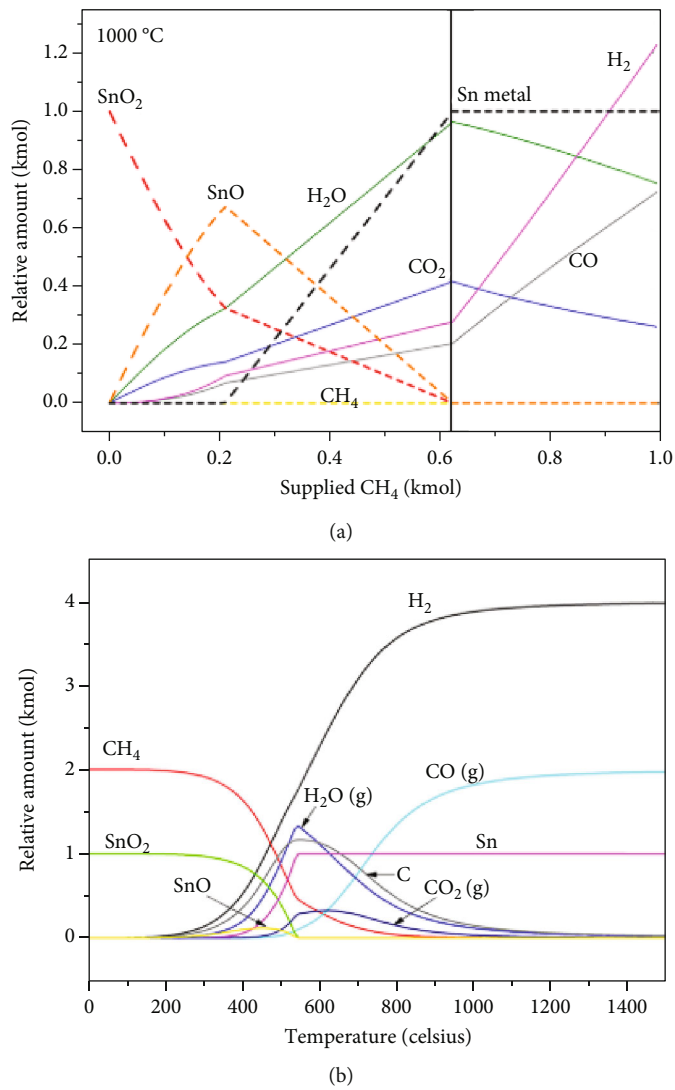


Figure 12: Theoretical prediction of the methane reduction of $SnO_2$. (a) Equilibrium concentration of the mixture of 1 kmol of $SnO_2$ and between 0 and 1 kmol of $CH_4$ at 1000°C as a function of the amount of supplied $CH_4$. (b) Temperature-dependent equilibrium relative concentration of a $SnO_2$-$CH_4$ mixture [107]. Reprinted with permission from Springer Nature. Copyright © 2017, Hyunwoo Ha et al.

## 3. Investigations on Practical Implementation of DRM in Liquid Metal and Molten Salt Reactors

Palmer et al. [17] performed a preliminary screening of different molten metal alloy catalysts in a bubble column. The conditions evaluated were residence time of ~1 s, temperature of 1080°C, total reactor pressure of 1 atm, and a stoichiometric feed of 2 : 1 $CH_4$ : $CO_2$. $CH_4$ and $CO_2$ conversion values obtained for the different alloys are summarized in Table 6.

They further studied dry reforming of methane in the 65 : 35 mol% Ni : In alloy and reported that the following reactions presented in Table 7 could take place.

Table 7 shows four reactions related to the molten metal used: $CH_4$ partial oxidation via $In_2O_3$, $CH_4$ oxidation via $In_2O_3$, $CO_2$ reduction via In, and $H_2$ oxidation via $In_2O_3$.

Table 6: $CH_4$ and $CO_2$ conversions obtained in a bubble column reactor filled with different molten metal alloys [17].

| Alloy | $XCH_4$ (%) | $XCO_2$ (%) |
|---|---|---|
| NiSn (25-75%) | 21 | 9.8 |
| FeSn (7-93%) | 24 | 11.3 |
| NiBi (33-67%) | 32 | 6.7 |
| NiIn (65-35%) | 44 | 81 |

Similar reactions may take place when using Sn as the liquid metal. For instance, it was found that $CO_2$ oxidizes the metal at temperatures above approximately 550°C [94]. As previously mentioned by Ha et al. [107], $CH_4$ provides a reducing atmosphere for $SnO_2$.

Figure 13 shows the results of the equilibrium calculations carried out at atmospheric pressure as a function of

Table 7: Potential reactions participating in the DRM in a 65 : 35 mol% Ni : In molten metal bubble column reactor [17].

| Eq. no. | Reaction | Chemical equation |
|---|---|---|
| (1) | Dry reforming of methane | $CH_4 + CO_2 \rightleftarrows 2H_2 + 2CO$ |
| (2) | Methane pyrolysis | $CH_4 \rightleftarrows 2H_2 + C_{(s)}$ |
| (3) | Steam methane reforming | $CH_4 + H_2O \rightleftarrows 3H_2 + CO$ |
| (4) | Reverse water-gas shift | $H_2 + CO_2 \rightleftarrows CO + H_2O$ |
| (5) | Reverse Boudouard | $CO_2 + C_{(s)} \rightleftarrows 2CO$ |
| (6) | Steam gasification of carbon | $H_2O + C_{(s)} \rightleftarrows CO + H_2$ |
| (7) | $CH_4$ partial oxidation via $In_2O_3$ | $CH_4 + (1/3)In_2O_3 \rightleftarrows 2H_2 + CO + (2/3)In$ |
| (8) | $CH_4$ oxidation via $In_2O_3$ | $CH_4 + (4/3)In_2O_3 \rightleftarrows 2H_2O + CO_2 + (8/3)In$ |
| (9) | $CO_2$ reduction via In | $CO_2 + (2/3)In \rightleftarrows CO + (1/3)In_2O_3$ |
| (10) | $H_2$ oxidation via $In_2O_3$ | $2H_2 + (2/3)In_2O_3 \rightleftarrows 2H_2O + (4/3)In$ |
| (11) | Dry reforming of methane + methane pyrolysis | $2CH_4 + 2CO_2 \rightleftarrows 4H_2 + 2CO + C$ |
| (12) | Autothermal reforming of methane | $4CH_4 + O_2 + 2H_2O \rightleftarrows 10H_2 + 4CO$ |
| (13) | Partial oxidation of methane | $2CH_4 + O_2 + CO_2 \rightleftarrows 3H_2 + 3CO + H_2O$ |

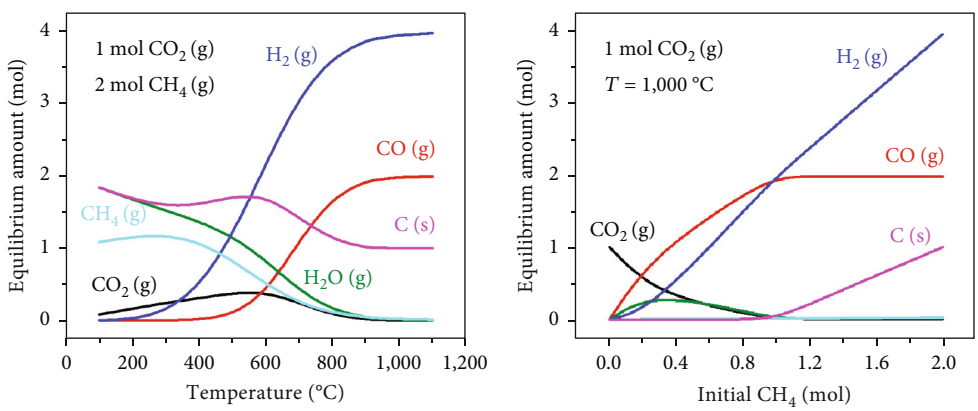


(a) (b)

Figure 13: Calculated equilibrium compositions of DRM at 1 atm. (a) 2 : 1 $CH_4 : CO_2$ molar ratio versus temperature and (b) 1 mol of $CO_2$ at 1000°C with differing initial moles of $CH_4$. Reprinted with permission from [17]. Copyright © 2020, Clarke Palmer et al., under exclusive licence to Springer Nature Limited.

the temperature and $CH_4/CO_2$ feed ratio based on the reactions reported in Table 7.

When $CH_4$ is used in excess at 1000°C, $CH_4$ and $CO_2$ are completely converted, there is no water if equilibrium is reached, and the $H_2 : CO$ product ratio can be increased at will by increasing the amount of $CH_4$.

They concluded that the advantages reached with this technology were as follows:

(1) The $H_2 : CO$ product ratio can be controlled by varying the $CH_4 : CO_2$ feed ratio

In particular, when using a 2 : 1 $CH_4 : CO_2$ ratio, the process produces a valuable syngas with high conversion and selectivity in a 2 : 1 $H_2 : CO$ ratio, which is immediately suitable for methanol synthesis and Fischer–Tropsch production of higher hydrocarbons. In the current implementation of dry reforming, one cannot use an excess of $CH_4$ because of coking, which limits the $H_2 : CO$ ratio in the product to 1 : 1.

(2) The process makes syngas by consuming $CO_2$, unlike SRM, which produces $CO_2$

(3) The solid carbon produced by the reaction floats to the surface of the melt where it can be removed

Yang et al. [66] presented a system comprising a liquid Ni-Bi alloy and a molten $K_2CO_3$ salt. The liquid alloy and the molten salt self-segregate into two layers inside a bubble column reactor, owing to density difference and immiscibility as shown in Figure 14, solving the coking and sintering issues of dry reforming. The conversions of $CH_4$ and $CO_2$ reached 60% and 70%, respectively, in a 30 cm bubble column comprising 15 cm $Ni_{0.27}Bi_{0.73}$ and 15 cm $K_2CO_3$ at 1050°C [66].

This 27% Ni-73% Bi alloy had been previously studied for methane pyrolysis. Upham et al. [75] achieved 95% methane conversion at 1065°C in a 1.1-meter-high bubble reactor. Rahimi et al. [109] employed the molten Ni-Bi alloy in combination with a molten salt (NaBr, KBr, or KCl) layer

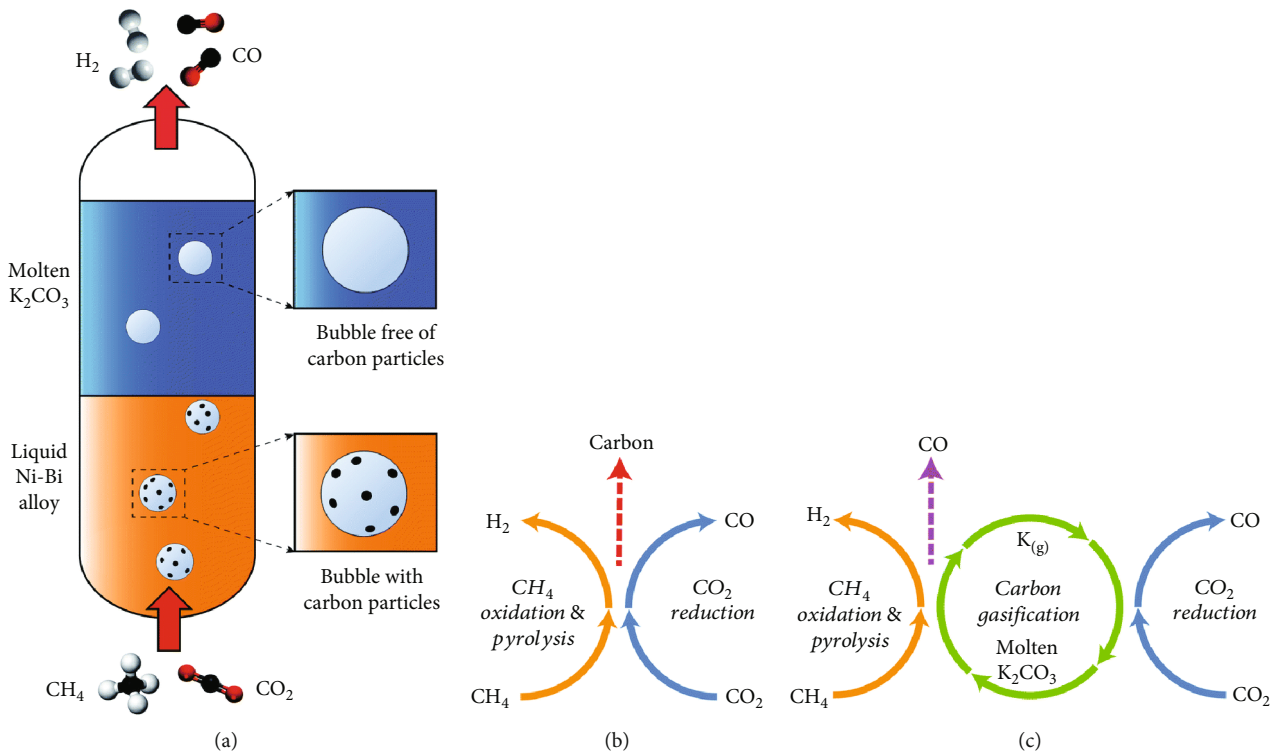


Figure 14: (a) Schematic of the bubble column reactor comprising a liquid Ni-Bi alloy layer and a molten $K_2CO_3$ layer, (b) reaction between $CH_4$ and $CO_2$ to produce $H_2$ and CO, (c) chemical loops for major reactions between $CH_4$ and $CO_2$ and $K_2CO_3$ in the liquid NiBi-$K_2CO_3$ catalytic system [66]. Used with permission of the Royal Society of Chemistry, from reference [66]; permission conveyed through the Copyright Clearance Center, Inc.

floating on the metal layer, added for removing contaminants from the carbon product.

Yang et al. [66] also performed dry-reforming experiments with 15 cm of only molten $Ni_{0.27}Bi_{0.73}$ for comparison. Results are shown in Figure 15 for experiments carried out with an inlet gas feed of $CH_4 : CO_2 = 1 : 1$ at a total flow rate of 10 $cm^3$/min.

CO selectivity (Figure 15(c)) was considerably lower in this case (reached a maximum value of ~70% at 1050°C) compared to the NiBi-$K_2CO_3$ system (near 100%). However, the $H_2$ selectivity achieved at 1050°C (approximately 90%) was similar in both dry-reforming processes performed. Furthermore, this value agrees with the results obtained by Upham et al. [75] for methane pyrolysis in molten NiBi with 95% $H_2$ selectivity at 1065°C.

It is worth noting that Yang et al. [66], while not analyzing in detail the formation of water vapor during reforming, mention that the other 10% hydrogen was converted to water (and KOH when molten $K_2CO_3$ is also used), which is removed by passing the gas product through a drying column installed before the gas chromatograph.

A $H_2$ : CO ratio in the gas product greater than unity was reported (Figure 15(d)), mainly attributable to the relatively low CO selectivity. The $H_2$ : CO ratio decreased with the increase of temperature mostly due to the promotion of the reverse Boudouard reaction at higher temperatures.

Kodama et al. [63] studied for $CO_2$ reforming of methane a molten $Na_2CO_3/K_2CO_3$ mixed salt containing a suspended metal catalyst powder at 950°C. Ni, Fe, Cu, or W metals on an $Al_2O_3$ support were examined for activity and selectivity, and the Ni/$Al_2O_3$ catalyst was found to be the most active and selective one. They observed as well that with higher $W/F$ ratios (where $W$ is the total weight of the molten salt bath and the Ni/$Al_2O_3$ catalyst mixture and $F$ is the flow rate of $CH_4$/$CO_2$ mixture), $CH_4$ conversion increased. Their results are plotted in Figure 16.

Experiments were carried out by varying $W$ between 30 and 50 g (in this case with a constant catalyst/molten salt weight ratio of 1) and $F$ between 200 and 800 $Ncm^3\,min^{-1}$. As can be seen in Figure 16, the methane conversion increased linearly with the $W/F$ ratio, and the $H_2$/CO ratio approached unity at higher $W/F$ values.

Based on the aforementioned limited experimental results available for dry reforming of methane in molten metal-filled reactors, it has been shown to be effective in the production of syngas with high conversion and selectivity. The choice of molten media, $CH_4/CO_2$ ratio, and operating temperature has a significant effect on the results obtained. This also determines the $H_2$ : CO ratio in the syngas product, which can be very interesting in terms of flexibility for a wide range of applications, making it an intriguing avenue for further exploration and optimization.

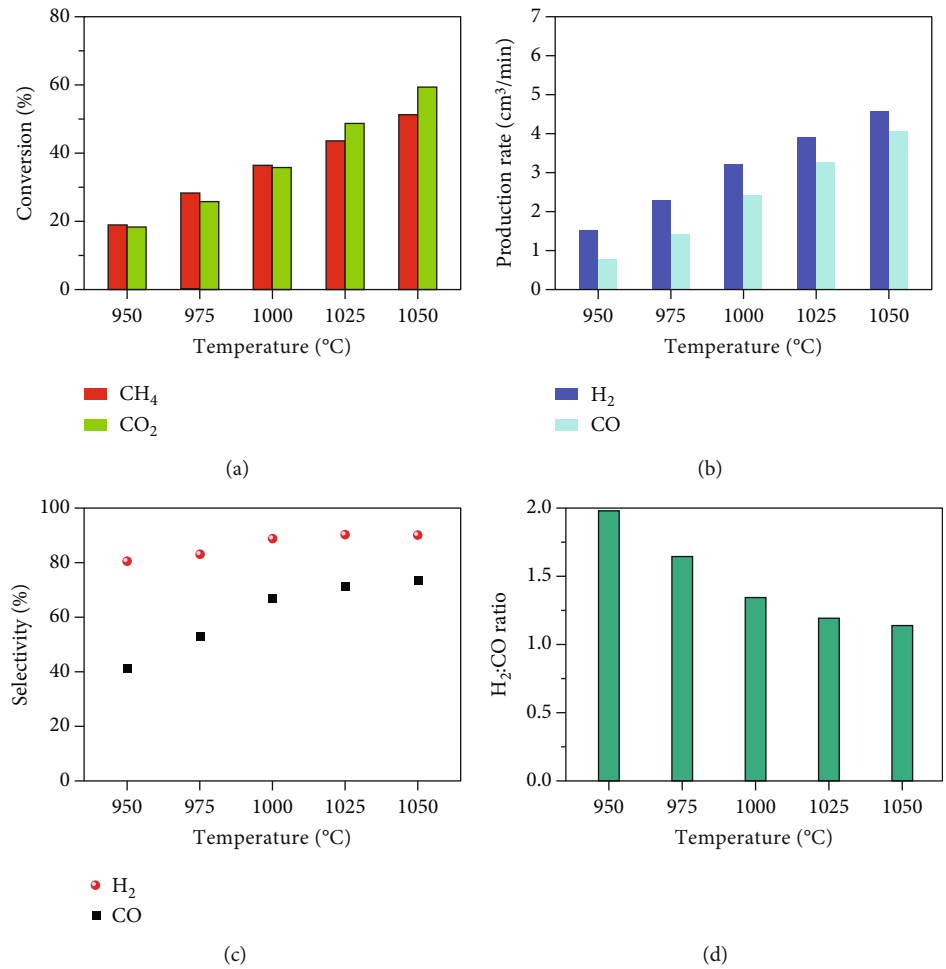


Figure 15: Dry reforming with liquid $Ni_{0.27}Bi_{0.73}$: (a) the conversions of $CH_4$ and $CO_2$, (b) the rates of producing $H_2$ and CO, (c) the selectivities of $H_2$ and CO, and (d) the $H_2$ : CO ratio in the gas product as a function of the temperature [66]. Used with permission of the Royal Society of Chemistry, from reference [66]; permission conveyed through the Copyright Clearance Center, Inc.

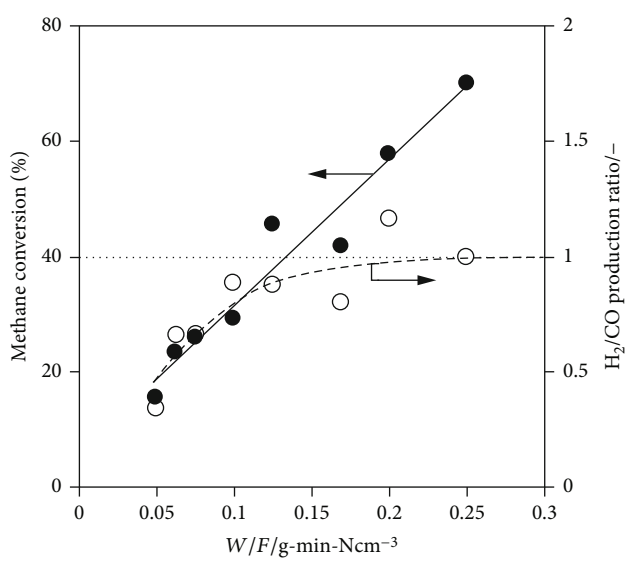


Figure 16: $CH_4$ conversion and $H_2$/CO ratio as a function of $W/F$, where $W$ and $F$ represent the weight of the $Ni/Al_2O_3$-carbonate mixture and the flow rate of the $CH_4/CO_2$ feed, respectively. $W$ and $F$ ranged from 30 to 50 g and 200-800 $Ncm^3\ min^{-1}$, respectively [63]. Reprinted with permission from [63]. Copyright © 2001, American Chemical Society.

Table 8: Main reactions in the dry reforming of biogas in a bubble column reactor filled with liquid tin.

| Name | Reaction |
|---|---|
| $CO_2$ reforming of methane | $CH_4 + CO_2 \rightleftarrows 2CO + 2H_2$ |
| $CH_4$ pyrolysis | $CH_4 \rightleftarrows C + 2H_2$ |
| Reverse water-gas shift | $CO_2 + H_2 \rightleftarrows CO + H_2O$ |
| Boudouard | $2CO \rightleftarrows CO_2 + C$ |
| Steam reforming of methane | $CH_4 + H_2O \rightleftarrows CO + 3H_2$ |
| Steam reforming of methane | $CH_4 + 2H_2O \rightleftarrows CO_2 + 4H_2$ |
| $CO_2$ oxidation of Sn | $Sn + 2CO_2 \rightleftarrows 2CO + SnO_2$ |
| $CH_4$ reduction of $SnO_2$ | $SnO_2 + 2CH_4 \rightleftarrows Sn + 4H_2 + 2CO$ |

## 4. Conclusions

Biogas is an interesting feedstock for the dry-reforming reaction due to its high $CO_2$ and $CH_4$ content. In this process, hydrogen is produced simultaneously by two reactions: dry reforming of methane and methane pyrolysis. The dry-reforming reaction is typically carried out at elevated temperatures above 800°C. In addition, other parallel reactions will occur simultaneously, including the reverse water-gas shift and the Boudouard reaction. In this case, carbon formation can take place mainly by two reactions depending on the process temperature: the Boudouard reaction and pyrolysis of methane. Using a liquid tin reactor, the carbon would float atop the surface due to the lower density of carbon compared to liquid tin.

While the use of liquid tin bubble column reactors for methane pyrolysis has already been tested, it is necessary to conduct a preliminary theoretical study of how the presence of $CO_2$ would affect the liquid tin in order to carry out DRM in such reactors. Although it is known that $CO_2$ could oxidize metal tin at temperatures above 550°C, several studies in the literature [17, 93, 105] have found that the tin oxide formed is in turn reduced back to Sn in the presence of carbon and methane. Therefore, under typical DRM operating conditions, irreversible formation of Sn oxides that might negatively affect the continuous system operation is unlikely. Moreover, neither tin carbides nor carbonates are expected to be formed. However, to confirm that, it would be useful to analyze the residues formed in the molten tin under DRM conditions operated over a long time.

According to available sources, the main reactions by dry reforming of methane (pyrolysis of biogas) in a liquid tin reactor, assuming that only $CO_2$ and $CH_4$ are present in the feed gas, are as listed in Table 8.

The composition of the product stream varies as a function of the amount of supplied $CH_4$ and $CO_2$ and of course the operating temperature. Thus, the $H_2/CO$ ratio in the gas product could be adjusted to some extent. For instance, methanol synthesis requires a 2 : 1 $H_2$ : CO ratio. Looking at this particular process, it should also be pointed out that the presence of water in the gas product could be a problem as it plays an important role in the deactivation of the catalysts [110] and may need to be removed.

It should be noted that the compositions predicted by all the equilibrium analyses found in the literature are still theoretical upper limits of the dry-reforming process, and the results may change in practice due to reaction kinetics.

In conclusion, assuming a biogas stream consisting of $CH_4$ and $CO_2$, the products to be obtained would be a gas mixture made up of mostly $H_2$, CO, and $CO_2$ (and maybe some water vapor) and a carbonaceous product. Traces of some intermediate component such as $C_2H_2$, $C_2H_4$, $C_2H_6$, $CH_3OH$, or $CH_2O$ could also be found.

The direct use of biogas for the reforming process eliminates the costly carbon dioxide separation step and has considerable environmental or climate protection potential. Further work should be carried out regarding the two main problems involved in dry reforming: carbon deposition and high energy requirements. As it is proposed here, the utilization of a liquid tin reactor would avoid the issue of carbon deposition and favor heat transfer. Moreover, the energy required to heat the reactor could be obtained from a renewable energy source as in solar reforming reactors [111, 112].

## Nomenclature

| | |
|---|---|
| ATR: | Autothermal reforming |
| bcm: | Billions of cubic meters |
| BECCS: | Bioenergy carbon capture and storage |
| Bi: | Bismuth |
| C: | Carbon |
| $CH_2O$: | Formaldehyde |
| $CH_3OCH_3$: | Dimethyl ether |
| $CH_3OH$: | Methanol |
| $CH_4$: | Methane |
| $C_2H_2$: | Acetylene |
| $C_2H_4$: | Ethylene |
| $C_2H_6$: | Ethane |
| Co: | Cobalt |
| CO: | Carbon monoxide |
| $CO_2$: | Carbon dioxide |
| $c_p$: | Specific heat capacity (kJ/kg K) |
| DME: | Dimethyl ether |
| DRM: | Dry reforming of methane |
| Fe: | Iron |
| g: | gaseous |
| Ga: | Gallium |
| $H_2$: | Hydrogen |
| $H_2O$: | Water |
| In: | Indium |
| K: | Equilibrium constant |
| $K_2CO_3$: | Potassium carbonate |
| KALLA: | Karlsruhe Liquid Metal Laboratory |
| KBr: | Potassium bromide |
| KCl: | Potassium chloride |
| KIT: | Karlsruhe Institute of Technology |
| Mn: | Manganese |
| NaBr: | Sodium bromide |
| $Na_2CO_3$: | Sodium carbonate |
| NET: | Negative Emissions Technologies |
| Ni: | Nickel |
| $O_2$: | Oxygen |
| P: | Pressure |
| Pb: | Lead |

RWGS: Reverse water-gas shift
s: Solid
Sn: Tin
SnO: Tin oxide or stannous oxide
$SnO_2$: Tin dioxide or stannic oxide
SRM: Steam reforming of methane
T: Temperature
TRM: Tri-reforming of methane
X: Conversion (%).

*Greek Letters*

$\Delta G_r$: Gibbs free energy of reaction (kJ/mol)
$\Delta H_r$: Enthalpy of reaction (kJ/mol)
$\Delta S_r$: Entropy (J/K mol)
$\lambda$: Thermal conductivity (W/m K)
$\rho$: Density (kg/m$^3$)
$\mu$: Dynamic viscosity (mPa/s).

## Data Availability

The data used to support the findings of this theoretical study are from previously reported studies, which are cited at relevant places within the text as references.

## Conflicts of Interest

The authors declare that they have no conflicts of interest.

## Acknowledgments

The Helmholtz Association of German Research Centres (HGF) and the Federal Ministry of Education and Research (BMBF), Germany, are gratefully acknowledged for their support of the Innovation Pool Project "Clean and Compressed Solar $H_2$" and the Helmholtz program "Materials and Technologies for the Energy Transition" (MTET). The publication is also funded by the Deutsche Forschungsgemeinschaft (DFG, 491111487). Open access funding was enabled and organized by Projekt DEAL.

## References

[1] EBA, "EBA statistical report," European Biogas Association, 2020, http://www.europeanbiogas.eu.

[2] S. Rasi, A. Veijanen, and J. Rintala, "Trace compounds of biogas from different biogas production plants," *Energy*, vol. 32, no. 8, pp. 1375–1380, 2007.

[3] X. Zhao, B. Joseph, J. Kuhn, and S. Ozcan, "Biogas reforming to syngas: a review," *iScience*, vol. 23, no. 5, article 101082, 2020.

[4] X. Chen, J. Jiang, K. Li, S. Tian, and F. Yan, "Energy-efficient biogas reforming process to produce syngas: the enhanced methane conversion by $O_2$," *Applied Energy*, vol. 185, pp. 687–697, 2017.

[5] A. Vita, L. Pino, F. Cipiti, M. Lagana, and V. Recupero, "Biogas as renewable raw material for syngas production by tri-reforming process over $NiCeO_2$ catalysts: optimal operative condition and effect of nickel content," *Fuel Processing Technology*, vol. 127, pp. 47–58, 2014.

[6] I. V. Yentekakis, G. Goula, P. Panagiotopoulou et al., "Dry reforming of methane: catalytic performance and stability of Ir catalysts supported on $\gamma$-Al2O3, Zr0.92Y0.08O2−$\delta$ (YSZ) or Ce0.9Gd0.1O2−$\delta$ (GDC)," *Topics in Catalysis*, vol. 58, pp. 1228–1241, 2015.

[7] X. Zhang, C. Yang, Y. Zhang, Y. Xu, S. Shang, and Y. Yin, "Ni-Co catalyst derived from layered double hydroxides for dry reforming of methane," *International Journal of Hydrogen Energy*, vol. 40, no. 46, pp. 16115–16126, 2015.

[8] R. Broun and M. Sattler, "A comparison of greenhouse gas emissions and potential electricity recovery from conventional and bioreactor landfills," *Journal of Cleaner Production*, vol. 112, pp. 2664–2673, 2016.

[9] R. del Valle-Zermeño, M. S. Romero-Güiza, J. M. Chimenos, J. Formosa, J. Mata-Alvarez, and S. Astals, "Biogas upgrading using MSWI bottom ash: an integrated municipal solid waste management," *Renewable Energy*, vol. 80, pp. 184–189, 2015.

[10] J. Díez-Ramírez, F. Dorado, A. Martínez-Valiente, J. M. García-Vargas, and P. Sánchez, "Kinetic, energetic and exergetic approach to the methane tri-reforming process," *International Journal of Hydrogen Energy*, vol. 41, no. 42, pp. 19339–19348, 2016.

[11] X. Fei, D. Zekkos, and L. Raskin, "Quantification of parameters influencing methane generation due to biodegradation of municipal solid waste in landfills and laboratory experiments," *Waste Management*, vol. 55, pp. 276–287, 2016.

[12] A. Vita, C. Italiano, C. Fabiano, M. Lagana, and L. Pino, "Influence of Ce-precursor and fuel on structure and catalytic activity of combustion synthesized $Ni/CeO_2$ catalysts for biogas oxidative steam reforming," *Materials Chemistry and Physics*, vol. 163, pp. 337–347, 2015.

[13] R. Chein and Z. W. Yang, "$H_2S$ effect on dry reforming of biogas for syngas production," *International Journal of Energy Research*, vol. 43, no. 8, pp. 3330–3345, 2019.

[14] IEA, "Outlook for biogas and biomethane. Prospects for organic growth. World Energy Outlook special report," 2020, https://www.iea.org/reports/outlook-for-biogas-and-biomethane-prospects-for-organic-growth.

[15] H. F. Coward and G. W. Jones, "Limits of inflammability of gases and vapors," *Journal of the Franklin Institute*, vol. 203, no. 1, p. 161, 1927.

[16] Marcogaz and European Biogas Association, *Biomethane: Responsibilities for Injection into Natural Gas Grid*, 2019.

[17] C. Palmer, D. C. Upham, S. Smart, M. J. Gordon, H. Metiu, and E. W. McFarland, "Dry reforming of methane catalysed by molten metal alloys," *Nature Catalysis*, vol. 3, no. 1, pp. 83–89, 2020.

[18] X. He and L. Liu, "Thermodynamic analysis on the $CO_2$ conversion processes of methane dry reforming for hydrogen production and $CO_2$ hydrogenation to dimethyl ether," *IOP Conference Series: Earth and Environmental Science*, vol. 100,, no. 1, 2017.

[19] P. Cao, S. Adegbite, and T. Wu, "Thermodynamic equilibrium analysis of $CO_2$ reforming of methane: elimination of carbon deposition and adjustment of $H_2$/CO ratio," *Energy Procedia*, vol. 105, pp. 1864–1869, 2017.

[20] D. Han, Y. Kim, W. Cho, and Y. Baek, "Effect of oxidants on syngas synthesis from biogas over 3 wt % Ni-Ce-MgO-$ZrO_2$/$Al_2O_2$ catalyst," *Energies*, vol. 13, no. 2, 2020.

[21] K. Wittich, M. Krämer, N. Bottke, and S. A. Schunk, "Catalytic dry reforming of methane: insights from model systems," *ChemCatChem*, vol. 12, no. 8, pp. 2130–2147, 2020.

[22] IEA Bioenergy, *Biogas Upgrading and Utilisation*, International Energy Agency, 2000.

[23] S. Abanades and M. Chambon, "$CO_2$ dissociation and upgrading from two-step solar thermochemical processes based on ZnO/Zn and $SnO_2$/SnO redox pairs," *Energy and Fuels*, vol. 24, no. 12, pp. 6667–6674, 2010.

[24] M. E. Gálvez, P. G. Loutzenhiser, I. Hischier, and A. Steinfeld, "$CO_2$ splitting via two-step solar thermochemical cycles with Zn/ZnO and FeO/$Fe_3O_4$ redox reactions: thermodynamic analysis," *Energy and Fuels*, vol. 22, no. 5, pp. 3544–3550, 2008.

[25] N. Abatzoglou and S. Boivin, "A review of biogas purification processes," *Biofuels, Bioproducts and Biorefining*, vol. 3, no. 1, pp. 42–71, 2009.

[26] E. Ryckebosch, M. Drouillon, and H. Vervaeren, "Techniques for transformation of biogas to biomethane," *Biomass and Bioenergy*, vol. 35, no. 5, pp. 1633–1645, 2011.

[27] C. Song and W. Pan, "Tri-reforming of methane: a novel concept for catalytic production of industrially useful synthesis gas with desired $H_2$/CO ratios," *Catalysis Today*, vol. 98, no. 4, pp. 463–484, 2004.

[28] R. Y. Chein and W. H. Hsu, "Analysis of syngas production from biogas via the tri-reforming process," *Energies*, vol. 11, no. 5, 2018.

[29] D. P. Minh, T. S. Phan, D. Grouse, and A. Nzihou, "Thermodynamic equilibrium study of methane reforming with carbon dioxide, water and oxygen," *Journal of Clean Energy Technologies*, vol. 6, no. 4, pp. 309–313, 2018.

[30] M. K. Nikoo and N. A. S. Amin, "Thermodynamic analysis of carbon dioxide reforming of methane in view of solid carbon formation," *Fuel Processing Technology*, vol. 92, no. 3, pp. 678–691, 2011.

[31] N. A. K. Aramouni, J. G. Touma, B. A. Tarboush, J. Zeaiter, and M. N. Ahmad, "Catalyst design for dry reforming of methane: analysis review," *Renewable and Sustainable Energy Reviews*, vol. 82, pp. 2570–2585, 2018.

[32] C.-J. Chen, M. H. Back, and R. A. Back, "The thermal decomposition of methane. I. Kinetics of the primary decomposition to $C_2H_6$ + $H_2$; rate constant for the homogeneous unimolecular dissociation of methane and its pressure dependence," *Canadian Journal of Chemistry*, vol. 53, no. 23, pp. 3580–3590, 1975.

[33] M. S. Khan and B. L. Crynes, "Survey of recent methane pyrolysis literature," *Industrial and Engineering Chemistry*, vol. 62, no. 10, pp. 54–59, 1970.

[34] J. M. Lavoie, "Review on dry reforming of methane, a potentially more environmentally-friendly approach to the increasing natural gas exploitation," *Frontiers in Chemistry*, vol. 2, p. 81, 2014.

[35] B. Abdullah, N. A. Abd Ghani, and D.-V. N. Vo, "Recent advances in dry reforming of methane over Ni-based catalysts," *Journal of Cleaner Production*, vol. 162, pp. 170–185, 2017.

[36] M. González-Castaño, B. Dorneanu, and H. Arellano-García, "The reverse water gas shift reaction: a process systems engineering perspective," *Reaction Chemistry & Engineering*, vol. 6, no. 6, pp. 954–976, 2021.

[37] I. Istadi and N. A. S. Amin, "Co-generation of $C_2$ hydrocarbons and synthesis gases from methane and carbon dioxide: a thermodynamic analysis," *Journal of Natural Gas Chemistry*, vol. 14, no. 3, pp. 140–150, 2005.

[38] K. Stangeland, H. Li, and Z. Yu, "Thermodynamic analysis of chemical and phase equilibria in $CO_2$ hydrogenation to methanol, dimethyl ether, and higher alcohols," *Industrial and Engineering Chemistry Research*, vol. 57, no. 11, pp. 4081–4094, 2018.

[39] S. Sharifian, M. Miltner, and M. Harasek, "Thermodynamic and kinetic based simulation approach to $CO_2$ and CO methane hydrogenation," *Chemical Engineering Transactions*, vol. 52, pp. 565–570, 2016.

[40] Ş. Özkara-Aydınoğlu, "Thermodynamic equilibrium analysis of combined carbon dioxide reforming with steam reforming of methane to synthesis gas," *International Journal of Hydrogen Energy*, vol. 35, no. 23, pp. 12821–12828, 2010.

[41] D. Pham Minh, T. J. Siang, D.-V. N. Vo et al., "Hydrogen production from biogas reforming: an overview of steam reforming, dry reforming, dual reforming, and tri-reforming of methane," in *Hydrogen Supply Chains*, pp. 111–166, Elsevier, 2018.

[42] B. J. Leal Pérez, J. A. Medrano Jiménez, R. Bhardwaj, E. Goetheer, M. van Sint Annaland, and F. Gallucci, "Methane pyrolysis in a molten gallium bubble column reactor for sustainable hydrogen production: proof of concept & techno-economic assessment," *International Journal of Hydrogen Energy*, vol. 46, no. 7, pp. 4917–4935, 2021.

[43] R. Y. Chein, Y. C. Chen, C. T. Yu, and J. N. Chung, "Thermodynamic analysis of dry reforming of $CH_4$ with $CO_2$ at high pressures," *Journal of Natural Gas Science and Engineering*, vol. 26, pp. 617–629, 2015.

[44] E. le Saché, A. Alvarez Moreno, and T. R. Reina, "Biogas conversion to syngas using advanced Ni-promoted pyrochlore catalysts: effect of the $CH_4$/$CO_2$ ratio," *Frontiers in Chemistry*, vol. 9, 2021.

[45] Y. Cui, H. Zhang, H. Xu, and W. Li, "Kinetic study of the catalytic reforming of $CH_4$ with $CO_2$ to syngas over Ni/$\alpha$-$Al_2O_3$ catalyst: the effect of temperature on the reforming mechanism," *Applied Catalysis A: General*, vol. 318, pp. 79–88, 2007.

[46] D. Pakhare and J. Spivey, "A review of dry ($CO_2$) reforming of methane over noble metal catalysts," *Chemical Society Reviews*, vol. 43, no. 22, pp. 7813–7837, 2014.

[47] S. Wang, G. Q. (. M.). Lu, and G. J. Millar, "Carbon dioxide reforming of methane to produce synthesis gas over metal-supported catalysts: state of the art," *Energy & Fuels*, vol. 10, no. 4, pp. 896–904, 1996.

[48] F. G. M. de Medeiros, F. W. B. Lopes, and B. Rego de Vasconcelos, "Prospects and technical challenges in hydrogen production through dry reforming of methane," *Catalysts*, vol. 12, no. 4, p. 363, 2022.

[49] S. Soleimani and M. Lehner, "Tri-reforming of methane: thermodynamics, operating conditions, reactor technology and efficiency evaluation—a review," *Energies*, vol. 15, no. 19, p. 7159, 2022.

[50] M. S. Challiwala, M. M. Ghouri, P. Linke, M. M. El-Halwagi, and N. O. Elbashir, "A combined thermo-kinetic analysis of various methane reforming technologies: comparison with dry reforming," *Journal of CO2 Utilization*, vol. 17, pp. 99–111,, 2017.

[51] Z. Bao and F. Yu, "Catalytic conversion of biogas to syngas via dry reforming process," in *Advances in Bioenergy*, pp. 43–76, Elsevier Inc., 2018.

[52] S. Praserthdam and P. B. Balbuena, "Performance evaluation of catalysts in the dry reforming reaction of methane via the ratings concept," *Reaction Kinetics, Mechanisms and Catalysis*, vol. 122, no. 1, pp. 53–68, 2017.

[53] O. Muraza and A. Galadima, "A review on coke management during dry reforming of methane," *International Journal of Energy Research*, vol. 39, no. 9, pp. 1196–1216, 2015.

[54] A. S. A. Al-Fatesh, A. H. Fakeeha, and A. E. Abasaeed, "Effects of selected promoters on Ni/Y-$Al_2O_3$ catalyst performance in methane dry reforming," *Chinese Journal of Catalysis*, vol. 32, no. 9–10, pp. 1604–1609, 2011.

[55] B. Djebarri, V. M. Gonzalez-Delacruz, D. Halliche et al., "Promoting effect of Ce and Mg cations in Ni/Al catalysts prepared from hydrotalcites for the dry reforming of methane," *Reaction Kinetics, Mechanisms and Catalysis*, vol. 111, no. 1, pp. 259–275, 2014.

[56] K. Takanabe, K. Nagaoka, K. Nariai, and K. I. Aika, "Titania-supported cobalt and nickel bimetallic catalysts for carbon dioxide reforming of methane," *Journal of Catalysis*, vol. 232, no. 2, pp. 268–275, 2005.

[57] D. San-José-Alonso, J. Juan-Juan, M. J. Illán-Gómez, and M. C. Román-Martínez, "Ni, Co and bimetallic Ni-Co catalysts for the dry reforming of methane," *Applied Catalysis A: General*, vol. 371, no. 1–2, pp. 54–59, 2009.

[58] S. Zeng, L. Zhang, X. Zhang, Y. Wang, H. Pan, and H. Su, "Modification effect of natural mixed rare earths on Co/$\gamma$-$Al_2O_3$ catalysts for $CH_4/CO_2$ reforming to synthesis gas," *International Journal of Hydrogen Energy*, vol. 37, no. 13, pp. 9994–10001, 2012.

[59] G. R. Moradi, M. Rahmanzadeh, and F. Khosravian, "The effects of partial substitution of Ni by Zn in $LaNiO_3$ perovskite catalyst for methane dry reforming," *Journal of CO2 Utilization*, vol. 6, pp. 7–11, 2014.

[60] B. Qiao, A. Wang, X. Yang et al., "Single-atom catalysis of CO oxidation using Pt1/FeOx," *Nature Chemistry*, vol. 3, no. 8, pp. 634–641, 2011.

[61] M. Usman, W. M. A. Wan Daud, and H. F. Abbas, "Dry reforming of methane: influence of process parameters—a review," *Renewable and Sustainable Energy Reviews*, vol. 45, pp. 710–744, 2015.

[62] A. Kumar, "Low temperature activation of carbon dioxide by ammonia in methane dry reforming—a thermodynamic study," *Catalysts*, vol. 8, no. 10, p. 481, 2018.

[63] T. Kodama, T. Koyanagi, T. Shimizu, and Y. Kitayama, "$CO_2$ reforming of methane in a molten carbonate salt bath for use in solar thermochemical processes," *Energy & Fuels*, vol. 15, no. 1, pp. 60–65, 2001.

[64] K. Al-Ali, S. Kodama, and H. Sekiguchi, "Modeling and simulation of methane dry reforming in direct-contact bubble reactor," *Solar Energy*, vol. 102, pp. 45–55, 2014.

[65] N. Gokon, Y. Oku, H. Kaneko, and Y. Tamaura, "Methane reforming with $CO_2$ in molten salt using FeO catalyst," *Solar Energy*, vol. 72, no. 3, pp. 243–250, 2002.

[66] Q. Yang, C. Zhou, J. Ni, and X. Guan, "Methane dry reforming in a coking- and sintering-free liquid alloy-salt catalytic system," *Sustainable Energy & Fuels*, vol. 4, no. 6, pp. 2768–2774, 2020.

[67] J. Pacio and T. Wetzel, "Assessment of liquid metal technology status and research paths for their use as efficient heat transfer fluids in solar central receiver systems," *Solar Energy*, vol. 93, pp. 11–22, 2013.

[68] U. Herrmann and D. W. Kearney, "Survey of thermal energy storage for parabolic trough power plants," *Journal of Solar-Energy Engineering*, vol. 124, no. 2, pp. 145–152, 2002.

[69] M. M. Kenisarin, "High-temperature phase change materials for thermal energy storage," *Renewable and Sustainable Energy Reviews*, vol. 14, no. 3, pp. 955–970, 2010.

[70] K. Niedermeier, L. Marocco, J. Flesch, G. Mohan, J. Coventry, and T. Wetzel, "Performance of molten sodium vs. molten salts in a packed bed thermal energy storage," *Applied Thermal Engineering*, vol. 141, pp. 368–377,, 2018.

[71] A. Heinzel, W. Hering, J. Konys et al., "Liquid metals as efficient high-temperature heat-transport fluids," *Energy Technology*, vol. 5, no. 7, pp. 1026–1036, 2017.

[72] M. Msheik, S. Rodat, and S. Abanades, "Experimental comparison of solar methane pyrolysis in gas-phase and molten-tin bubbling tubular reactors," *Energy*, vol. 260, article 124943, 2022.

[73] A. Abánades, R. K. Rathnam, T. Geißler et al., "Development of methane decarbonisation based on liquid metal technology for $CO_2$-free production of hydrogen," *International Journal of Hydrogen Energy*, vol. 41, no. 19, pp. 8159–8167, 2016.

[74] N. Zaghloul, S. Kodama, and H. Sekiguchi, "Hydrogen production by methane pyrolysis in a molten-metal bubble column," *Chemical Engineering and Technology*, vol. 44, no. 11, pp. 1986–1993, 2021.

[75] D. C. Upham, V. Agarwal, A. Khechfe et al., "Catalytic molten metals for the direct conversion of methane to hydrogen and separable carbon," *Science*, vol. 358, no. 6365, pp. 917–921, 2017.

[76] C. Palmer, M. Tarazkar, H. H. Kristoffersen et al., "Methane pyrolysis with a molten Cu-Bi alloy catalyst," *ACS Catalysis*, vol. 9, no. 9, pp. 8337–8345, 2019.

[77] J. Li, Y. Xie, K. Zeng et al., "Biomass gasification in molten salt for syngas production," *Energy*, vol. 210, p. 118563, 2020.

[78] D. Kang, N. Rahimi, M. J. Gordon, H. Metiu, and E. W. McFarland, "Catalytic methane pyrolysis in molten $MnCl_2$-KCl," *Applied Catalysis B: Environmental*, vol. 254, pp. 659–666, 2019.

[79] C. Palmer, M. Tarazkar, M. J. Gordon, H. Metiu, and E. W. McFarland, "Methane pyrolysis in low-cost, alkali-halide molten salts at high temperatures," *Sustainable Energy & Fuels*, vol. 5, no. 23, pp. 6107–6123, 2021.

[80] C. F. Patzschke, B. Parkinson, J. J. Willis et al., "Co-Mn catalysts for $H_2$ production via methane pyrolysis in molten salts," *Chemical Engineering Journal*, vol. 414,, article 128730, 2021.

[81] D. Kang, C. Palmer, D. Mannini et al., "Catalytic methane pyrolysis in molten alkali chloride salts containing iron," *ACS Catalysis*, vol. 10, no. 13, pp. 7032–7042, 2020.

[82] J. Boo, E. H. Ko, N. K. Park et al., "Methane pyrolysis in molten potassium chloride: an experimental and economic analysis," *Energies*, vol. 14, no. 23, 2021.

[83] B. Parkinson, C. F. Patzschke, D. Nikolis, S. Raman, D. C. Dankworth, and K. Hellgardt, "Methane pyrolysis in monovalent alkali halide salts: kinetics and pyrolytic carbon properties," *International Journal of Hydrogen Energy*, vol. 46, no. 9, pp. 6225–6238, 2021.

[84] L. Stoppel, T. Fehling, T. Geißler, E. Baake, and T. Wetzel, "Carbon dioxide free production of hydrogen," *IOP Conference Series: Materials Science and Engineering*, vol. 228, no. 1, article 012016, 2017.

[85] T. Geißler, A. Abánades, A. Heinzel et al., "Hydrogen production via methane pyrolysis in a liquid metal bubble column reactor with a packed bed," *Chemical Engineering Journal*, vol. 299, pp. 192–200, 2016.

[86] A. Uihlein, *Analyse des Einflusses von $CO_2$-haltigem Eduktgas auf die Herstellung von Carbon Black Partikeln mittels Methanpyrolyse*, 2020.

[87] M. A. Pimenta, G. Dresselhaus, M. S. Dresselhaus, L. G. Cançado, A. Jorio, and R. Saito, "Studying disorder in graphite-based systems by Raman spectroscopy," *Physical Chemistry Chemical Physics*, vol. 9, no. 11, pp. 1276–1290, 2007.

[88] G. Ding, Y. Zhu, S. Wang et al., "Chemical vapor deposition of graphene on liquid metal catalysts," *Carbon*, vol. 53, pp. 321–326, 2013.

[89] J. C. Minx, W. F. Lamb, M. W. Callaghan et al., "Negative emissions - part 1: research landscape and synthesis," *Environmental Research Letters*, vol. 13, no. 6, 2018.

[90] S. Fuss, W. F. Lamb, M. W. Callaghan et al., "Negative emissions - part 2: costs, potentials and side effects," *Environmental Research Letters*, vol. 13, no. 6, 2018.

[91] G. F. Nemet, M. W. Callaghan, F. Creutzig et al., "Negative emissions—part 3: innovation and upscaling," *Environmental Research Letters*, vol. 13, no. 6, article 063003, 2018.

[92] M. Epstein, I. Vishnevetsky, and A. Berman, "The $SnO_2$/Sn carbothermic cycle for splitting water and production of hydrogen," *Journal of Solar Energy Engineering*, vol. 132, no. 3, pp. 0310071–0310077, 2010.

[93] R. Padilla and H. Y. Sohn, "The reduction of stannic oxide with carbon," *Metallurgical Transactions B*, vol. 10, no. 1, pp. 109–115, 1979.

[94] R. N. Lyon, *Liquid-Metals Handbook*, 1954.

[95] R. E. A. Eatwell-Hall, V. N. Sharifi, and J. Swithenbank, "Hydrogen production from molten metal gasification," *International Journal of Hydrogen Energy*, vol. 35, no. 24, pp. 13168–13178, 2010.

[96] O. Ruff and B. Bergdahl, "Arbeiten im gebiet hoher temperaturen. XII. Die messung von dampfspannungen bei sehr hohen temperaturen nebst einigen beobachtungen über die löslichkeit von kohlenstoff in metallen," *Zeitschrift für anorganische und allgemeine Chemie*, vol. 106, no. 1, pp. 76–94, 1919.

[97] Dechema eV, *Werkstofftechnische Maßnahmen zur Reduzierung der Abscheidung von Kohlenstoff auf Anlagenbauteilen durch die Blockierung der katalytischen Wirkung von Werkstoffoberflächen*, 2013.

[98] U. Heubner and A. Melin, *Gase und Kohlenstoff in Metallen*, 1976.

[99] L. L. Oden and N. A. Gokcen, "Sn-C and Al-Sn-C phase diagrams and thermodynamic properties of C in the alloys: 1550 °C to 2300 °C," *Metallurgical Transactions B*, vol. 24, no. 1, pp. 53–58, 1993.

[100] J. R. Anderson, *Solubility of carbon in molten copper-manganese and copper-nickel alloys, [Ph.D. thesis]*, Massachusetts Institute of Technology, 1946.

[101] T. Y. Kosolapova, *Carbides*, Springer US, Boston, MA, USA, 1995.

[102] L. L. Oden, "Phase equilibria in the Al-Fe-C system: isothermal sections 1550 °C to 2300 °C," *Metallurgical Transactions A*, vol. 20, no. 12, pp. 2703–2706, 1989.

[103] J. C. Platteeuw and G. Meyer, *The system tin + oxygen*, Department of General and Inorganic Chemistry, Technical University Delft, 1955.

[104] P. Charvin, S. Abanades, F. Lemont, and G. Flamant, "Experimental study of $SnO_2$/SnO/Sn thermochemical systems for solar production of hydrogen," *AICHE Journal*, vol. 54, no. 10, pp. 2759–2767, 2008.

[105] G. Levêque and S. Abanades, "Thermodynamic and kinetic study of the carbothermal reduction of $SnO_2$ for solar thermochemical fuel generation," *Energy & Fuels*, vol. 28, no. 2, pp. 1396–1405, 2014.

[106] S. Abanades, "$CO_2$ and $H_2O$ reduction by solar thermochemical looping using $SnO_2$/SnO redox reactions: thermogravimetric analysis," *International Journal of Hydrogen Energy*, vol. 37, no. 10, pp. 8223–8231, 2012.

[107] H. Ha, M. Yoo, H. An et al., "Design of reduction process of $SnO_2$ by $CH_4$ for efficient Sn recovery," *Scientific Reports*, vol. 7, 2017.

[108] T. M. Emmerich, *Materialwissenschaftliche Aspekte der Methanzersetzung in flüssigem Zinn*, 2018.

[109] N. Rahimi, D. Kang, J. Gelinas et al., "Solid carbon production and recovery from high temperature methane pyrolysis in bubble columns containing molten metals and molten salts," *Carbon*, vol. 151, pp. 181–191, 2019.

[110] R. Peláez, E. Bryce, P. Marín, and S. Ordóñez, "Catalyst deactivation in the direct synthesis of dimethyl ether from syngas over CuO/ZnO/Al2O3 and $\gamma$-Al2O3 mechanical mixtures," *Fuel Processing Technology*, vol. 179, pp. 378–386, 2018.

[111] C. Agrafiotis, H. von Storch, M. Roeb, and C. Sattler, "Solar thermal reforming of methane feedstocks for hydrogen and syngas production—a review," *Renewable and Sustainable Energy Reviews*, vol. 29, pp. 656–682, 2014.

[112] E. J. Sheu, E. M. A. Mokheimer, and A. F. Ghoniem, "A review of solar methane reforming systems," *International Journal of Hydrogen Energy*, vol. 40, no. 38, pp. 12929–12955, 2015.